





Lindblad master equation approach to the topological phase transition in the disordered Su-Schrieffer-Heeger model

Andrea Nava ^{1,2}, Gabriele Campagnano ³, Pasquale Sodano ⁴, and Domenico Giuliano ^{1,2}

¹*Dipartimento di Fisica, Università della Calabria Arcavacata di Rende I-87036, Cosenza, Italy*

²*I.N.F.N., Gruppo Collegato di Cosenza, Arcavacata di Rende I-87036, Cosenza, Italy*

³*CNR-SPIN, Complesso Monte S. Angelo-Via Cintia, I-80126, Napoli, Italy*

⁴*I.N.F.N., Sezione di Perugia, Via A. Pascoli, I-06123, Perugia, Italy*



(Received 24 October 2022; revised 15 December 2022; accepted 19 December 2022; published 10 January 2023)

We use the Lindblad equation method to investigate the onset of a mobility edge and the topological phase transition in the disordered SSH chain connected to two external baths in the large bias limit. From the scaling properties of the nonequilibrium stationary current flowing across the system, we recover the localization/delocalization in the disordered chain. To probe the topological phase transition in the presence of disorder, we use the even-odd differential occupancy as a means to discriminate topologically trivial from topologically nontrivial phases in the out-of-equilibrium system. Eventually, we argue how to generalize our method to other systems undergoing a topological phase transition in the presence of disorder.

DOI: [10.1103/PhysRevB.107.035113](https://doi.org/10.1103/PhysRevB.107.035113)

I. INTRODUCTION

A common way to discriminate between different phases of matter is by looking at their symmetries. Ordered phases are typically characterized by a lower level of symmetry than disordered ones. In many cases, this allows for introducing an order parameter as the average value of a local observable, which is different from (equal to) zero in an ordered (disordered) phase. Such an approach does not apply to topological phase transitions.

The concept of a topological phase has been originally introduced within the theoretical investigation of the quantum Hall effect [1], as a phase not characterized by any symmetry-breaking mechanism but rather by fundamental topological properties that are insensitive to smooth changes in the quantum state of the system [2–4].

Topological phases are also of remarkable interest for practical applications, as all of them are characterized by nontrivial edge or surface states, which, being protected by the topology of the phase itself, have potential applications ranging from spintronics to topological quantum computation [5]. It is, therefore, of the utmost importance to have a criterion to distinguish topologically nontrivial phases from topologically trivial ones. Despite that, it is, in general, not simple to select a physical quantity playing the role of an order parameter at a topological phase transition.

For lattice models that are translationally invariant by finite, lattice step translations, the key quantity sensible to topology is the Chern number, defined as the integral of the Berry curvature over the Brillouin zone of the system [6,7]. By definition, the Chern number is a collective property of the state of the system that must be an integer: It is naturally quantized and cannot be altered by a smooth deformation of the state which does not alter its global topological properties. It is either zero, or different from zero, depending on whether

the system is topologically trivial or not. In one-dimensional systems, the Chern number is proportional to the charge polarization, which measures the end charge of the system, Q_{end} [7–10]. Q_{end} is different from zero provided the system hosts a nontrivial edge state and, therefore, it is sensible to whether the system is in a topologically trivial or nontrivial state [7].

When computed in a one-dimensional system, it corresponds to the Zak phase [8], that is, to the integral of the Berry connection over a closed path transversing the whole Brillouin zone. Importantly enough, nowadays technology already allows for a direct measurement of the Zak phase in cold atoms on optical lattices [11], with a good perspective of soon being able to perform similar measurements in solid-state devices.

In real systems, one has to face the unavoidable presence of the disorder due to impurities and/or defects. In particular, in one dimension, uncorrelated disorder typically leads to full localization of the electronic wave functions and to the corresponding suppression of the current transport [12,13]. In the specific context of topological materials, disorder can lead to reentrant topological phases [14–16], with the corresponding onset of disorder-induced topological Anderson insulators [17]. Moreover, in the presence of correlated disorder, such as the random bond [18] or the random dimer disorder [19], the interplay of disorder and topology can give rise to phases with remarkable properties, which are presently the subject of an intense research activity, on the theoretical [16,20–22], as well as on the experimental side, in solid-state systems, as well as in cold atom systems [23–25].

Over all, the largest part of the theoretical, as well as of the experimental research, has been focused onto the Su-Schrieffer-Heeger (SSH) model for polyacetylene [26]. This is motivated on one hand by the fact that, despite its apparent simplicity, the theoretical model of SSH is able to catch the relevant physics arising from the interplay between topology

and disorder, and on the other hand by the relative ease to experimentally realize the model in setups like, e.g., GaAs-AlGaAs superlattices [27], 1D waveguide array fabricated in fused silica [28], or one-dimensional two-component ultracold atomic mixtures in an optical lattice [25].

Investigating the phase diagram of the disordered SSH model presents two relevant kinds of difficulties. First, even in the absence of disorder, the SSH model is insulating. This implies that, when investigating the disorder-induced delocalization-localization phase transition, one cannot rely on the suppression of linear electric conductance as a function of the system size, since charge transport is already suppressed by the gap, even in the clean limit. Moreover, disorder breaks the lattice translational invariance, which invalidates the calculation of most of the quantities usually employed to distinguish the topologically nontrivial phase from the topologically trivial one.

In this paper, we apply the Lindblad master equation (LE) formalism [29] to investigate both the localization-delocalization transition and the topological transition in a disordered open SSH chain connected to two external reservoirs (the baths) in the large bias limit between the baths. The LE approach allows us to model, on very general grounds, the Markovian dynamics of an open quantum system connected to one or several baths. In recent years, it has played a crucial role in different contexts, such as ultracold atoms [30,31], condensed matter systems [32–36], quantum biology, and quantum chemistry [37–40], with the possibility to implement quantum algorithms and experimentally realize Markovian dynamics [41–44]. Furthermore, the Lindblad approach has recently been used to induce topological phase transitions, in one- and two-dimensional systems, leading to another universality class of Anderson transitions [45–48]. In the context of quasi-one-dimensional systems, the LE has been used to investigate both relaxation dynamics toward a thermal state, in terms of localized, or extended, bulk Lindblad operators [49–53], as well as the nonequilibrium steady states (NESSs) that emerge when a system is placed in contact with two reservoirs at different temperatures or voltage bias/chemical potentials [54–61].

In our specific case, the baths connected to the SSH chain play the role of particle source and sink reservoirs and are modeled as Lindblad local operators. Holding the baths at the large bias limit drives the system toward a NESS that is characterized by a steady-state value of the charge current, I_{NESS} . As we rigorously prove analytically and evidence numerically, I_{NESS} is finite in the absence of disorder, despite the system being gapped. Roughly speaking, this is due to the fact that I_{NESS} is determined by states at all the energies, including, in particular, the conducting ones above the gap. Disorder-induced localization of the states determines a suppression of I_{NESS} as a consequence of the corresponding localization of single-particle wave functions. This eventually makes $I_{\text{NESS}} \rightarrow 0$ the chain length $L \rightarrow \infty$ whenever all the single-particle states are localized. Following this observation, we identify the localized/delocalized phases of our system according to whether I_{NESS} is suppressed/keeps finite as $L \rightarrow \infty$.

We therefore evidence how once, in the large bias limit, the chain is taken to a specific NESS, the even-odd differential

occupancy (EOD) can be efficiently used to probe the nontrivial topological properties of the NESS itself. Specifically, by combining analytical and numerical methods, we show how a value of the EOD of about ± 1 is directly related to the existence of the in-gap states that characterize the topological phase, both in the clean limit and in the presence of (bond or dimer) disorder. We therefore conclude that our LE approach to the disordered, open SSH chain allows us to encompass at the same time both the localization/delocalization transition, as well as the topological properties of the system, which eventually allows us to map out the corresponding phase diagram with respect to both physical properties. Eventually, after proving the effectiveness of our method, we argue how it can be potentially extended to disordered physical systems with nontrivial topological properties other than the SSH chain.

The paper is organized as follows:

(1) In Sec. II, we introduce the model Hamiltonian for the SSH chain in the clean limit and analyze the two different types of disorder we consider here. Moreover, we present the LE approach and how we apply it to our system.

(2) In Sec. III, we derive the I_{NESS} both in the clean limit and in the presence of disorder. In particular, we show how to map out the localization/delocalization phase transition from the behavior of I_{NESS} as L gets large.

(3) In Sec. IV, we introduce the EOD as a collective property of the NESS and show how to use it to probe the topologically nontrivial/trivial nature of the out-of-equilibrium state.

(4) In Sec. V, we summarize our results and provide possible further developments of our paper.

(5) In Appendix A, we outline the derivation of the Eq. (14) of the main text, while in Appendix B we review the solution of the SSH model over a finite chain with open boundary conditions in the absence of disorder, as well as the calculation of the scattering amplitudes in the presence of an impurity in the chain.

II. MODEL AND METHODS

In the following, we introduce the Hamiltonian for the one-dimensional SSH model [26] and present the Lindblad equation approach, which we employ to drive the system toward a NESS and to measure the physical quantities we use to characterize the phase diagram of the model, in the clean limit as well as in the presence of disorder.

A. Model Hamiltonian

Over a one-dimensional, L -site lattice, the Hamiltonian of the SSH model is given by [26]

$$H_{\text{SSH}} = - \sum_{j=1}^{L-1} J_{j,j+1} \{c_j^\dagger c_{j+1} + c_{j+1}^\dagger c_j\} - \sum_{j=1}^L \mu_j c_j^\dagger c_j \quad . \quad (1)$$

In Eq. (1), we, respectively, denote with c_j, c_j^\dagger the annihilation and the creation operator for a single spinless fermion at site j of the lattice, obeying the standard anticommutation algebra $\{c_j, c_j^\dagger\} = \delta_{j,j}$. With $J_{j,j+1}$ and μ_j we, respectively, denote the single-fermion hopping amplitude between site j

and site $j + 1$ and the chemical potential at site j . In the absence of impurities, we set $\mu_j = 0$ throughout the whole lattice, while for the $J_{j,j+1}$, consistently with the onset of dimerization in real polyacetylene in the presence of Peierls instability [26], we set

$$J_{j,j+1} = \begin{cases} J_o, & \text{for } j \text{ odd} \\ J_e, & \text{for } j \text{ even.} \end{cases} \quad (2)$$

Assuming periodic boundary conditions and for $\mu_j = 0 \forall j$, the SSH model undergoes a topological phase transition as a function of J_o/J_e . This corresponds to the (quantized) Berry phase associated to the occupied Bloch wave functions to switch from 0 to a finite value ($= \pi \bmod 2\pi$) [8,9].

The physical consequences of the topological phase transition are evidenced through the properties of the single-particle spectrum in the chain with open boundary conditions— H_{SSH} in Eq. (1)—as a function of L . Specifically, due to the Lieb theorem for dimerized systems [62,63], if L is odd the system has at least a zero-energy state at any values of J_o/J_e . In this case, H_{SSH} is symmetric under $J_o \leftrightarrow J_e$ and no topological transition appears at any value of J_o/J_e . At variance, for L even, two splitted in-gap states emerge in the single-particle spectrum for $J_o < J_e$ with opposite values of the energy. These two states correspond to a polarization charge $\pm e/2$ at the boundary of the chain [26]: They become strictly degenerate only in the thermodynamic limit, $L \rightarrow \infty$, in which case it is possible to linearly combine the corresponding wave functions into two orthogonal ones localized in real space near by either boundary of the chain. Due to this, from now on we shall assume L even throughout our paper.

In the following, we investigate the effects of two different kinds of disorder: The bond and the dimer disorder. To induce bond disorder, we assign to the odd bond coupling strength J_o a value randomly selected between $J_o = 1$ and $J_o = 1 - W$, with a binary probability distribution $\mathcal{P}_b[J_o]$ given by

$$\mathcal{P}_b[J_o] = \sigma \delta(J_o - 1) + (1 - \sigma) \delta(J_o - 1 + W), \quad (3)$$

so, at each odd bond of the chain, we may have single electron hopping J_o either equal to 1 or to $1 - W$, with probability, respectively, given by σ and $1 - \sigma$. Clearly, the $W = 0$ limit corresponds to the clean case. To induce the dimer disorder, we randomly assign to the chemical potential at both sites of each elementary cell (that is, two consecutive odd and even sites) either one of two selected values, of which one is set at 0 [16,64]. The corresponding probability distribution $\mathcal{P}_d[\mu]$ is given by

$$\mathcal{P}_d[\mu_j] = \begin{cases} \sigma \delta(\mu - 0) + (1 - \sigma) \delta(\mu - W) & j \text{ odd} \\ \mu_{j-1} & j \text{ even,} \end{cases} \quad (4)$$

so μ can be zero or W with probability σ and $1 - \sigma$, respectively. The $W = 0$ limit corresponds again to the clean case.

The two realizations of the disorder in Eqs. (3) and (4) have completely different physical consequences on the SSH chain due to the different behavior of the corresponding potential under the action of the chiral operator Γ defined as

$$\Gamma = \sum_{j=1}^{\frac{L}{2}} \{c_{2j-1}^\dagger c_{2j-1} - c_{2j}^\dagger c_{2j}\}. \quad (5)$$

In the clean limit, one has $\{\Gamma, H_{\text{SSH}}\} = 0$, provided that the chemical potential is set to 0, which leaves the spectrum of H_{SSH} invariant. When disorder is added to the SSH chain, thus breaking lattice translational invariance, it is no more possible to define the Berry phase as the integral over the Brillouin zone of the Berry connection. However, if the disordered Hamiltonian, at any given realization of the disorder potential, still anticommutes with Γ , it is possible to introduce a disorder-averaged real space winding number (DAWN), δ_v , which can be used to label topological phases in the presence of disorder.

Specifically, in a one-dimensional system of length L , δ_v is computed by ensemble averaging over a large enough number N of independent realizations of the disorder, according to the formula [21,65]

$$\delta_v = \frac{1}{N} \sum_{s=1}^N \frac{1}{L} \text{Tr}\{\Gamma Q_s [Q_s, X]\}. \quad (6)$$

In Eq. (6) s labels a single realization of the disorder, $Q_s = \sum_n \{|\psi_{n,s}\rangle \langle \psi_{n,s}| - \Gamma |\psi_{n,s}\rangle \langle \psi_{n,s}| \Gamma$, with $\{|\psi_{n,s}\rangle\}$ being a complete set of eigenfunctions of the Hamiltonian at the realization of the disorder labeled with s , and X being the unit-cell coordinate operator, $X = \text{diag}(1, 1, 2, 2, \dots, \frac{L}{2}, \frac{L}{2})$.

Due to the missing anticommutativity with Γ , the DAWN cannot be defined in the presence of dimer disorder. This requires introducing alternative means to investigate the combined effects of topology and disorder [16,64]. To bypass this limitation, in the following we define and employ the EOD. We show that our method allows us to witness the onset of topological phases in the presence of disorder regardless of whether the Hamiltonian anticommutes with Γ or not. Moreover, in the large bias limit, we show how our method can be equally well applied to equilibrium, as well as to out-of-equilibrium, open systems.

To analyze the disorder-induced localization effects on the electronic states of the system, we study the stationary charge transport properties of the open chain connected to two external baths taken at large chemical potential bias. Within the LE approach, we derive the stationary density matrix ρ describing the NESS that asymptotically sets in the system. Computing the corresponding stationary current I_{NESS} flowing through the chain, we will be able to spell out disorder-induced effects in the system through their effects in I_{NESS} . Motivated by this observation, we now present the main features of the LE approach to the SSH model.

B. Lindblad equation

The LE master equations consists of a first-order differential equation for the time evolution of the system density matrix $\rho(t)$, given by

$$\dot{\rho}(t) = -i[H, \rho(t)] + \sum_k \left(L_k \rho(t) L_k^\dagger - \frac{1}{2} \{L_k^\dagger L_k, \rho(t)\} \right). \quad (7)$$

The first term on the right-hand side of Eq. (7), called the Liouvillian, describes the unitary evolution determined by the system Hamiltonian H , while the second term, the Lindbladian, includes dissipation and decoherence on the system dynamics, with the jump operators L_k that are determined by

the coupling between the system and the baths. Throughout the following derivation, we assume $H = \sum_{i,j=1}^L c_i^\dagger \mathcal{H}_{i,j}(t) c_j$, with c_j, c_j^\dagger being the single-fermion creation and annihilation operators at site j and the Hamiltonian matrix elements $\mathcal{H}_{i,j}(t)$ which, in general, can depend on time t , as well.

In the following, we consider baths that locally inject (or extract) fermions to (from) the boundary sites of the chain, at given and fixed rates. We describe the injecting and extracting baths at site $j = \{1, L\}$ in terms of the Lindblad operators $L_{in,j}$ and $L_{out,j}$, given by

$$L_{in,j} = \sqrt{\Gamma_j} c_j^\dagger, \quad L_{out,j} = \sqrt{\gamma_j} c_j, \quad (8)$$

with Γ_j and γ_j being the coupling strengths, respectively, determining the creation and the annihilation of a fermion at site j .

We have a total of four, in principle, independent, coupling strengths, $\Gamma_1, \gamma_1, \Gamma_L$, and γ_L , that describe the coupling between the chain and the baths. When recovering the above couplings from the microscopic theory, we see that they can be expressed in terms of the Fermi distribution function at the chemical potential of the reservoir, f , and of the reservoir spectral density at the chemical potential of the reservoir, g . Specifically, we obtain [66,67]

$$\Gamma_j = g_j f_j, \quad \gamma_j = g_j(1 - f_j), \quad (9)$$

with (labeling each reservoir with the index of the site it is connected to) $j = \{1, L\}$.

In this paper, we focus on the large bias regime, which corresponds to setting $f_1 = 1$ and $f_L = 0$. In this limit, the reservoir coupled to site 1 acts as an electron source by only injecting electrons in the chain, and the reservoir coupled to site L acts as an electron drain by only absorbing electrons from the system. As a result, a steady-state current is induced due to electrons that enter the chain at site 1 and travel all the way down to site L , where they exit the chain. To derive the current in the large bias limit, we first determine $\rho(t)$ by solving Eq. (7). Then, we compute the (time-dependent) expectation value of any observable O , $O(t)$ using

$$O(t) = \text{Tr}[O\rho(t)]. \quad (10)$$

Taking into account Eq. (10) we employ Eq. (7) to write the LE directly for $O(t)$, obtaining

$$\begin{aligned} \frac{d}{dt} O(t) &= \text{Tr}(O\dot{\rho}(t)) \\ &= i\text{Tr}[[H, O]\rho(t)] + \sum_k \left(\text{Tr}[L_k^\dagger O L_k \rho(t)] \right. \\ &\quad \left. - \frac{1}{2} \text{Tr}[\{L_k^\dagger L_k, O\}\rho(t)] \right). \end{aligned} \quad (11)$$

In the following, we focus on the average value of the occupation number at a generic site i of the system, $n_j(t) = \text{Tr}[n_j \rho(t)]$, as well as of the currents flowing from the reservoirs into site $j = \{1, L\}$, $I_{in,j}(t)$ or from site $j = \{1, L\}$ to the reservoir, $I_{out,j}(t)$. These are given by

$$I_{in,j}(t) = \Gamma_j(1 - n_j(t)), \quad I_{out,j}(t) = \gamma_j n_j(t), \quad (12)$$

so the net current exchanged at time t between the reservoirs and site j is given by $I_j(t) = I_{in,j}(t) - I_{out,j}(t)$. In addition, we also need to derive the average value of the current flowing

between two connected sites of the chain, say, j and $j \pm 1$, $I_{j,j\pm 1}$. This is given by

$$I_{j,j\pm 1}(t) = -iJ_{j,j\pm 1} \mathcal{I}_{j,j\pm 1}(t) + \text{c.c.}, \quad (13)$$

with $\mathcal{I}_{j,j\pm 1}(t) = \text{Tr}[c_j^\dagger c_{j\pm 1} \rho(t)]$ and with c.c. denoting the complex conjugate.

The full set of LEs for $n_j(t)$, $I_{in,j}(t)$, $I_{out,j}(t)$, and $I_{j,j\pm 1}(t)$ allows us to recover the current across the chain when it is connected to external reservoirs. For a quadratic Hamiltonian, it is possible to write a closed set of equations for the bilinear operators only that can be written in matrix form as

$$\dot{\mathcal{C}}(t) = i[\mathcal{H}^\top(t), \mathcal{C}(t)] + \mathcal{G} - \frac{1}{2}\{(\mathcal{G} + \mathcal{R}), \mathcal{C}(t)\}, \quad (14)$$

with the bilinear expectation matrix elements $[\mathcal{C}(t)]_{i,j} = \text{Tr}[c_i^\dagger c_j \rho(t)]$ and the system-bath coupling matrix elements $[\mathcal{G}]_{i,j} = \delta_{i,j}(\delta_{j,1}\Gamma_1 + \delta_{j,L}\Gamma_L)$ and $[\mathcal{R}]_{i,j} = \delta_{i,j}(\delta_{j,1}\gamma_1 + \delta_{j,L}\gamma_L)$. The system evolves in time, asymptotically flowing to the NESS, which is determined from the condition $\dot{\mathcal{C}}(t) = 0$ (details about the derivation of Eq. (14) are provided in Appendix A).

In the following, we use Eq. (14) to describe the SSH model with different kinds of correlated disorder.

III. CURRENT AND STATE LOCALIZATION IN THE NONEQUILIBRIUM STEADY STATE

The most effective way of probing the disorder-induced localization in one-dimensional systems is through dc current transport measurements [68]. However, due to the presence of the dimerization gap, the SSH chain is insulating even in the absence of disorder. In this case, as an alternative (to transport properties) means to study the localization transition, it has been proposed to look at the normal- and inverse-participation ratios. These two quantities can directly be computed from the wave functions for the single-electron states in the system. By averaging over N -independent realizations of the disorder, they are, respectively, defined as [21]

$$\begin{aligned} \text{NPR} &= \frac{1}{N} \sum_{s=1}^N \frac{1}{L} \sum_n \left(L \sum_{j=1}^L |\langle j | \psi_{n,s} \rangle|^4 \right)^{-1}, \\ \text{IPR} &= \frac{1}{N} \sum_{s=1}^N \frac{1}{L} \sum_n \sum_{j=1}^L |\langle j | \psi_{n,s} \rangle|^4. \end{aligned} \quad (15)$$

As $L \rightarrow \infty$, either $\text{NPR} = 0$, corresponding to localization of all the states, or $\text{IPR} = 0$, corresponding to all the states being delocalized.

As we show in the following, driving the chain to the large-bias limit allows for using charge transport to probe the localization transition even for the insulating system. Indeed, in the linear response regime the current is proportional to the zero-energy transmission coefficient \mathcal{T} across the chain and is therefore exponentially suppressed with L as $e^{-\frac{L}{\xi}}$, with $\xi = 1/\tanh^{-1}[\frac{|J_c - J_d|}{J_c + J_d}]$. Instead, once the system is driven toward the NESS corresponding to the optimal working point by tuning the chain-bath coupling strength [59,60], I_{NESS} keeps finite as $L \rightarrow \infty$ even if the system is gapped.

On turning on the disorder, I_{NESS} is suppressed due to the strong localization effect of random disorder in

one-dimensional systems [12,13], thus signaling the onset of the delocalization/localization transition in the electronic states in the chain. Moreover, as we show below, I_{NESS} is also sensible to the onset of the mobility edge that has been predicted to arise, under suitable conditions, in one-dimensional disordered systems in the presence of correlated disorder and/or of structured impurities [19,64,69,70] (see also Ref. [71] for an extension to a two-leg ladder and Ref. [72] for a proposal of a practical implementation within an N -leg ladder realized with an optical lattice): the mobility edge is indeed naturally revealed by I_{NESS} maintaining a finite value, even on increasing L toward the scaling limit. Thus, we conclude that measuring I_{NESS} is enough to determine the localization/delocalization transition in our system. At variance, to discriminate between the topologically trivial and the topologically nontrivial phase, below we introduce the EOD as a suitable tool to infer the topological properties of the NESS.

To effectively ascertain the physical behavior of our system and how it is affected, in the following we employ analytical and numerical methods, by complementing one another, whenever possible.

A. I_{NESS} in the clean limit

In the absence of disorder, we compute I_{NESS} by employing the approach of Ref. [54]. The basic idea is to think of a three-region system: regions A and C , respectively, connected to the left- and to right-hand baths, and the central region B , whose sites are not directly connected to a bath and to eventually assume that A and C are weakly coupled to B . Defining g to be the small parameter controlling the coupling strength, so $0 < g \ll 1$, we compute the current to leading order in g .

The constraint over g does not affect the reliability of the final result (at least qualitatively). This is due to the absence of a bulk interaction in the SSH model, which makes the intersite hopping between neighboring a marginal boundary operator. Therefore, tuning its strength by continuously varying g toward the $g \rightarrow 1$ limit (which corresponds to our specific case) does not qualitatively alter the results we obtain in the small- g limit (note that this does not typically happen in the case in which g is the interaction strength in front of a relevant, or of a marginally relevant, boundary interaction, such as, for instance, in the presence of Majorana modes at the endpoints of the chain [73–75] or in the two-impurity Kondo model in a spin chain [76]).

In the following, we realize the single-site A and C regions by weakening the first and last bond of H_{SSH} in Eq. (1), according to

$$J_{1,2} = J_o \rightarrow gJ_o, \quad J_{L-1,L} = J_o \rightarrow gJ_o. \quad (16)$$

In Fig. 1, we provide a schematic drawing of our system, with the red arrow evidencing the particle injection from the source to the chain (with coupling Γ_1) and the green arrow corresponding to the particle injection from the chain into the drain (with coupling γ_L) when the system is taken to the large bias regime. The corresponding Hamiltonian \hat{H} is determined by the sum of the Hamiltonian of the two sites connected with the external baths, \hat{H}_A, \hat{H}_C , plus the terms coupling A and C sites to the middle chain, $\hat{V}_{A,B}$ and $\hat{V}_{B,C}$, plus the Hamiltonian

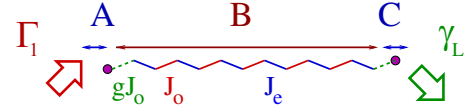


FIG. 1. Sketch of the SSH chain connected to one-site Lindblad baths (drawn as full, purple dots) with weakened bonds $J_{1,2} = J_{L-1,L} = gJ_o$ (drawn in green). In the figure, we evidence the three regions of length A , B , and C (see main text for details). The red arrow evidences the particle injection from the source to the chain (with coupling Γ_1) and the green arrow corresponds to the particle injection from the chain into the drain (with coupling γ_L) when the system is taken to the large bias regime.

for the middle region \hat{H}_B , that is,

$$\hat{H} = \hat{H}_A + \hat{H}_C + \hat{H}_B + \hat{V}_{A,B} + \hat{V}_{B,C}. \quad (17)$$

Using the notation α, α^\dagger and β, β^\dagger to, respectively, denote the single fermion annihilation and creation operators over, respectively, the first and last sites of the chain, we have

$$\hat{H}_A = \epsilon_\alpha \alpha^\dagger \alpha, \quad \hat{H}_C = \epsilon_\beta \beta^\dagger \beta,$$

$$\hat{H}_B = - \sum_{j=1}^{L-3} J_{j,j+1} \{c_j^\dagger c_{j+1} + c_{j+1}^\dagger c_j\},$$

$$\hat{V}_{A,B} = -gJ_o \{\alpha^\dagger c_1 + c_1^\dagger \alpha\}, \quad \hat{V}_{B,C} = -gJ_o \{\beta^\dagger c_L + c_L^\dagger \beta\}, \quad (18)$$

with $\epsilon_\alpha, \epsilon_\beta$ eventually sent to 0, consistently with Ref. [54] and with $J_{1,2} = J_e, J_{2,3} = J_o$, etc. Let us note that \hat{H}_B corresponds to the Hamiltonian of an SSH chain of $\hat{L} \equiv L - 2$ sites where J_e and J_o are exchanged with each other.

From Eqs. (18), we find that I_{NESS} is given by

$$I_{\text{NESS}} = - \frac{igJ_o}{2} \{ \langle \alpha^\dagger c_1 - c_1^\dagger \alpha \rangle - \langle \beta^\dagger c_L - c_L^\dagger \beta \rangle \}, \quad (19)$$

with $\langle \dots \rangle$ denoting the average of the operator on the NESS. To implement the perturbative expansion in g , we now introduce the eigenmodes of \hat{H}_B with energy $\lambda \epsilon_k$ ($\lambda = \pm$), $\Gamma_{\alpha,\lambda}$, which are given by

$$\Gamma_{k,\lambda} = \sum_{j=1}^{\hat{L}} (\psi_{j,k,\lambda})^* c_j, \quad \Gamma_{0,\lambda} = \sum_{j=1}^{\hat{L}} (\psi_{j,0,\lambda})^* c_j, \quad (20)$$

with the wave functions $\psi_{j,k,\pm}, \psi_{j,0,\pm}$, respectively, provided in Eqs. (B13) and (B17). The in-gap eigenmodes $\Gamma_{0,\lambda}$ are present, or not, depending on whether the chain is in the topological or the trivial, phase. Inverting Eqs. (20), we obtain

$$c_j = \sum_k \sum_\lambda \psi_{j,k,\lambda} \Gamma_{k,\lambda}. \quad (21)$$

Equation (21) allows us to express the right-hand side of Eq. (19) in terms of the matrix elements of the covariance matrix θ [54], according to

$$\begin{aligned} \langle \alpha^\dagger c_1 \rangle &= \sum_{k,\lambda} \psi_{1,k,\lambda} \langle \alpha^\dagger \Gamma_{k,\lambda} \rangle = \sum_k \sum_\lambda \psi_{1,k,\lambda} \theta_{\alpha;(k,\lambda)}, \\ \langle \beta^\dagger c_L \rangle &= \sum_k \sum_\lambda \psi_{L,k,\lambda} \langle \beta^\dagger \Gamma_{k,\lambda} \rangle = \sum_{k,\lambda} \psi_{L,k,\lambda} \theta_{\beta;(k,\lambda)}. \end{aligned} \quad (22)$$

The leading nonzero contribution to the right-hand side of Eqs. (22) arises to first order in g and is given by

$$\begin{aligned}\theta_{\alpha;(k,\lambda)} &= \frac{ig\psi_{1,k,\lambda}(\bar{f}_{\alpha} - \bar{f}_{k,\lambda})}{\gamma - i\lambda\epsilon_k}, \\ \theta_{\beta;(k,\lambda)} &= \frac{ig\psi_{L,k,\lambda}(\bar{f}_{\beta} - \bar{f}_{k,\lambda})}{\gamma - i\lambda\epsilon_k},\end{aligned}\quad (23)$$

with \bar{f}_{α} and \bar{f}_{β} denoting the Fermi distribution functions describing, respectively, the left- and right-hand bath-level occupancies within the NESS. To recover the large bias regime in the zero-temperature limit, we have to assume a negative (positive) chemical potential μ_{α} (μ_{β}) for the left-hand (right-hand) bath, respectively. This eventually implies $\bar{f}_{\alpha} = 1$, $\bar{f}_{\beta} = 0$. With $\bar{f}_{k,\lambda}$, we denote the distribution function of the modes of the chain within the NESS. Due to the symmetry of H_{SSH} under the replacement $j \leftrightarrow L + 1 - j$, we obtain $[\psi_{1,k,\lambda}]^2 = [\psi_{L,k,\lambda}]^2$, $\forall k, \lambda$. In this case, our analogs of Eqs. (53) and (54) of Ref. [54] are trivially solved by $\bar{f}_{k,\lambda}^{\text{SSH}} = \frac{1}{2}(\bar{f}_{\alpha} + \bar{f}_{\beta}) = \frac{1}{2}$, independent of k and λ . Finally, the particle-hole symmetry of the SSH chain at half filling implies $[\psi_{1,k,+}]^2 = [\psi_{1,k,-}]^2$ and $\epsilon_{k,+} = -\epsilon_{k,-}$. Collecting the above results all together, and noting that when the full system is in the topological phase the subsystem \hat{H}_B is in the trivial one, the steady-state current in the NESS in the topological phase is given by

$$I_{\text{NESS}} = \sum_{0 < k \leq \frac{\pi}{2}} \frac{\gamma g^2 J_o^2 [\psi_{1,k,-}]^2}{\gamma^2 + \epsilon_k^2}, \quad (24)$$

with the sum taken over the values of k that satisfy Eq. (B12) with $J_e \leftrightarrow J_o$ and no contribution to the current arising from the localized, subgap modes. To access the trivial phase, we simply use again Eq. (24), with just J_e and J_o exchanged with each other, thus getting

$$I_{\text{NESS}} = \sum_{0 < k \leq \frac{\pi}{2}} \frac{\gamma g^2 J_e^2 [\psi_{1,k,-}]^2}{\gamma^2 + \epsilon_k^2}, \quad (25)$$

with the sum over k now computed over the solutions of the secular equation corresponding to propagating states (real k), as well as over the localized mode solution, corresponding to $k = \frac{\pi}{2} - iq$, with q real and positive.

In Fig. 2, we plot I_{NESS} computed in an SSH chain with $L = 20$ sites with the analytical formulas in Eqs. (24) and (25) (red curve), as well as numerically calculated directly within the LE approach (blue curve) by keeping J_o fixed at 1 (reference energy value) and $\gamma/J_o = 1.5$ and by varying J_e , for $0 \leq J_e/J_o \leq 2$. In general, I_{NESS} shows a maximum I_M , as a function of J_e/J_o , at the topological phase transition, corresponding to the closure of the bulk gap of the chain at $J_e/J_o = 1$. To get rid of the arbitrary parameter g in Eqs. (24) and (25), in drawing both curves we normalize I_{NESS} at the corresponding value of I_M . We note the excellent agreement with each other, which evidences the due consistency between the analytical and the fully numerical approach. We also note that I_{NESS} keeps finite at any finite value of J_e/J_o .

To rule out the possibility that (as it happens when considering equilibrium dc transport throughout the SSH chain) this might be some finite-size effect, below we provide a general

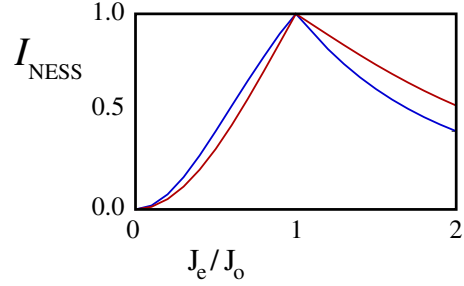


FIG. 2. I_{NESS} in an SSH chain with $L = 20$ as a function of J_e/J_o at fixed $J_o = 1$ and $\gamma/J_o = 1.5$, computed using the analytical expression in Eqs. (24) and (25) (red curve) and by direct implementation of the Lindblad equation approach (blue curve). In both cases, I_{NESS} has been normalized so it is equal to 1 for $J_e/J_o = 1$ (see main text for the corresponding discussion).

argument proving that, at any finite values of J_e and J_o and in the absence of disorder, I_{NESS} keeps finite as $L \rightarrow \infty$.

To do so, we show that Eqs. (24) and (25) are bounded from below and from above by two quantities that remain finite in the thermodynamic limit. Indeed, we note that, as $L \rightarrow \infty$, Eqs. (24) and (25) yield

$$I_{\text{NESS}} \approx \frac{L}{4\pi} \int_{-\pi}^{\pi} dk \left\{ \frac{\gamma g^2 \mathcal{J}^2}{\gamma^2 + \epsilon_k^2} \frac{[1 - \cos(2kL)]}{L - \frac{\sin(kL)\cos[k(L+2)]}{\sin(2k)}} \right\}, \quad (26)$$

with $\mathcal{J} = \min\{J_o, J_e\}$. From Eq. (26), we readily find that

$$\frac{3}{(3\pi + 1)} \mathcal{I}_L \leq I_{\text{NESS}} \leq \mathcal{I}_L, \quad (27)$$

with

$$\begin{aligned}\mathcal{I}_L &= \frac{\gamma g^2 \mathcal{J}^2}{2\pi} \int_{-\pi}^{\pi} dk \left\{ \frac{[1 - \cos(2kL)]}{\gamma^2 + \epsilon_k^2} \right\} \\ &= \gamma g^2 \mathcal{J}^2 \left\{ \frac{1 - z_*^L}{2\sqrt{(J_e^2 + J_o^2 + \gamma^2)^2 - 4J_e^2 J_o^2}} \right\},\end{aligned}\quad (28)$$

with

$$z_* = -\frac{J_e^2 + J_o^2 + \gamma^2}{2J_e J_o} + \sqrt{\frac{(J_e^2 + J_o^2 + \gamma^2)^2 - 4J_e^2 J_o^2}{4J_e^2 J_o^2}}. \quad (29)$$

Eventually, Eqs. (28) and (29) imply that, as $L \rightarrow \infty$, we get

$$\mathcal{I}_{L \rightarrow \infty} = \left\{ \frac{\gamma g^2 \mathcal{J}^2}{2\sqrt{(J_e^2 + J_o^2 + \gamma^2)^2 - 4J_e^2 J_o^2}} \right\}, \quad (30)$$

which is always finite at any finite values of J_e and J_o . Due to disorder-induced localization, the situation fully changes as disorder is turned on, though, as we discuss next, strongly depending on the nature of the disorder.

B. I_{NESS} and disorder-induced localization in the presence of bond disorder

In a one-dimensional conductor, any amount of disorder would lead to complete localization of single electron states and to the corresponding suppression of long-distance charge transport in the scaling limit [12,13]. At variance, disorder induced by correlated impurities with a nontrivial internal structure can give rise to a mobility edge that marks a metal-to-insulator transition, even in one-dimensional disordered conductors [19,64,69]. This is due to the fact that, differently from what happens with a structureless impurity located at a lattice site, an impurity with an internal structure, such as a correlated dimer, allows, under pertinent conditions on the values of the various system parameters, for a single-particle tunneling through, with zero reflection amplitude and just a total phase shift in the wave function [19].

That being stated, following standard arguments [77], one concludes that a chain of length L hosts a number of localized states $N_{\text{loc}} \sim \sqrt{L}$. These states support conduction, though, in the thermodynamic limit, they determine a zero-measure set. The disappearance of these states marks the metal-to-insulator phase transition. As we argue here and in the following section, the current I_{NESS} provides an effective way to detect the mobility edge in the disordered SSH chain [78].

To check where, and under what conditions, the mobility edge should arise in our system, we follow the main argument of Ref. [19], for both bond- and dimer-correlated disorder. Specifically, we derive the explicit expression for the reflection coefficient in the presence of the impurity, r_k , as a function of the momentum k and verify if, and under what conditions, $r_k = 0$, which marks the onset of the mobility edge [19]. In Appendix B, we derive r_k in the SSH chain in the presence of a bond and of a dimer impurity. In the case of a bond impurity, we find that r_k is given by

$$r_k = \frac{e^{Aik+i\varphi_k} W(2-W)}{-1 + e^{2i(k+\varphi_k)}(1-W)^2}. \quad (31)$$

Equation (31) implies that, *regardless of k* , we can recover the condition $r_k = 0$ only if either $W = 0$ (which corresponds to the trivial case of absence of disorder, or $W = 2$. In the scaling limit, we therefore expect that bond disorder induces full localization of the electronic states, except along the lines in parameter space corresponding to $W = 0$ and $W = 2$ (note that r_k is symmetric under $W \leftrightarrow 2W$, so we do expect a corresponding symmetry for the phase diagram).

To evidence how this reflects in the behavior of I_{NESS} , we have used the LE approach to compute it in the presence of bond disorder, as a function of W/J_0 and of the ratio J_e/J_0 (using J_0 as unit of energy and accordingly setting it to 1) for increasing values of L . To account for the disorder, at each set of values of J_e/J_0 , W and L , we ensemble averaged the results for I_{NESS} over $N = 50$ realizations of the bond disorder, with probability of having a single altered bond set at $1 - \sigma = 0.5$. To optimize our procedure by letting the system operate at the optimal working point by maximizing I_{NESS} , we repeated the procedure of Ref. [60] and eventually chose $\gamma = 2$.

In Fig. 3, we draw our result for I_{NESS} as a function of W/J_0 and of J_e/J_0 , for $0 \leq W \leq 2.5$ and for $0 \leq J_e/J_0 \leq 2$, in a chain at increasing values of $L = 20, 40, 80$ connected to two

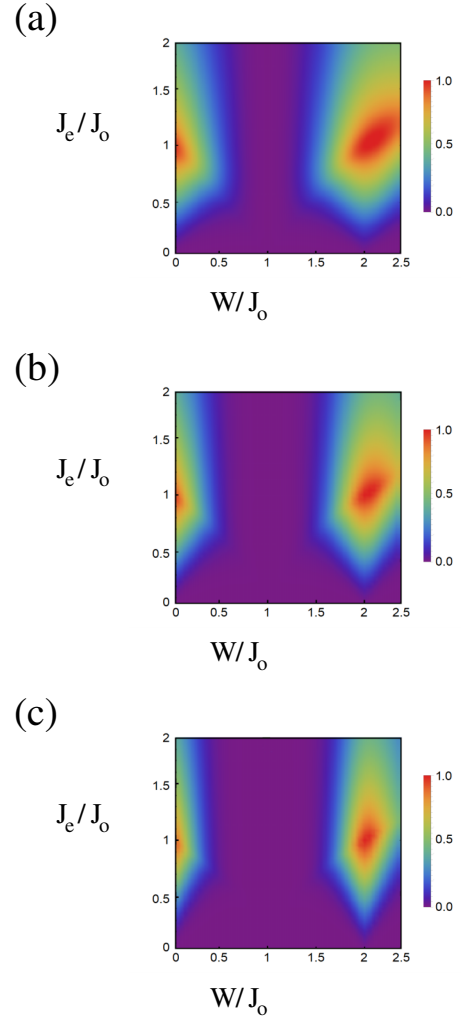


FIG. 3. (a) I_{NESS} in an $L = 20$ SSH chain with bond disorder in the hopping terms with $\sigma = 0.5$ [see Eq. (3)], as a function of W/J_0 and of J_e/J_0 , for $0 \leq W/J_0 \leq 2.5$ and for $0 \leq J_e/J_0 \leq 2$ (J_0 has been used as a reference energy and it has therefore been set to 1). The figure has been generated by averaging over $N = 50$ different realizations of the bond disorder. The couplings to the Lindblad baths have been set so $\Gamma_1 = \gamma_L = \gamma = 2$. The color code highlights the value of I_{NESS} (normalized at its maximum) as evidenced in the figure. (b) Same as in (a) but with $L = 40$. (c) Same as in (a) but with $L = 80$.

Lindblad baths in the large-bias regime, with couplings to the bath $\Gamma_1 = \gamma_L \equiv \gamma$. From the color code for the value of I_{NESS} we see that, on one hand, the current is maximal over regions centered on the lines $W/J_0 = 0, 2$, which is consistent with the criterion of Ref. [19] and with the result of Eq. (B25). Moving across Figs. 3(a)–3(c), we also see that, as expected, the larger the L , the more the region in parameter space over which I_{NESS} is appreciably $\neq 0$ shrinks over the lines $W/J_0 = 0, 2$. Anywhere else, the system is insulating as $L \rightarrow \infty$.

As an independent cross-check of our conclusions, in Fig. 4 we plot I_{NESS} computed with the same parameters we used to draw Fig. 3, but at a single realization of the disorder, as a function of L for $20 \leq L \leq 160$, with $J_e/J_0 = 1.5$ and for $W/J_0 = 0, 0.1, 0.25$. We clearly see that, while there is

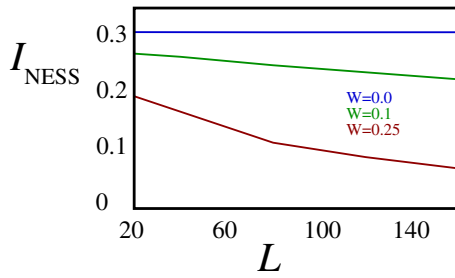


FIG. 4. I_{NESS} as a function of L for $20 \leq L \leq 160$ computed in a SSH chain with $J_e/J_o = 1.5$, with couplings to the Lindblad baths set so $\Gamma_1 = \gamma_L = \gamma = 2$ at a given realization of bond disorder, with $W = 0.0$ (blue line), $W = 0.1$ (green line), and $W = 0.25$ (red line).

apparently no scaling at all (as it must be) for $W/J_o = 0$, in both the other cases I_{NESS} appears to scale toward 0 on increasing L . We therefore conclude that, as $L \rightarrow \infty$, the bond disorder suppresses I_{NESS} everywhere in parameter space, except along the vertical lines $W = 0$ and $W = 2$.

C. I_{NESS} and disorder-induced localization in the presence of dimer disorder

As we show in Appendix B, the reflection amplitude r_k across a dimer impurity is given by

$$r_k = -\frac{e^{4ik+i\varphi_k} W (W + 2J_o \cos(k + \varphi_k))}{J_o^2 + 2e^{i(k+\varphi_k)} J_o W + e^{2i(k+\varphi_k)} (-J_o^2 + W^2)}. \quad (32)$$

From Eq. (32), we now see that $r_k = 0$ if either $W = 0$ (which, again, corresponds to the trivial limit of absence of disorder) or $W + 2J_o \cos(k + \varphi_k) = 0$. This latter condition corresponds to the result of Ref. [19] for a dimer impurity, once one, respectively, identifies ϵ_a and V of that paper with our W and J_o , and once one notes that, in our case, we have set ϵ_b of Ref. [19] at 0 and have an additional contribution φ_k in the argument of the cosine that disappears, once one sets $J_e = J_o$, as in Ref. [19].

The equation $W + 2J_o \cos(k + \varphi_k) = 0$ takes a solution k_* for $0 \leq k \leq \pi$ only provided that $|W/2J_o| \leq 1$. If this is the case, over an L -site chain, \sqrt{L} electronic states (out of the total of L states) centered around k_* are not localized by the disorder and, though, as $L \rightarrow \infty$, they contribute the total number of states by a zero measure set, they are nevertheless enough to support a conducting phase in the chain, thus determining the onset of a mobility edge [19,69].

To evidence how this affects I_{NESS} , we have generalized Eqs. (24) and (25) to the case in which a single impurity is present in the chain. In this case, due to the lack of symmetry of the system under the site-order inversion, $j \leftrightarrow L - j + 1$, Eqs. (24) and (25) are substituted by

$$I_{\text{NESS}} = \sum_{0 \leq k \leq \frac{\pi}{2}} \left\{ \frac{2\gamma g^2 \mathcal{J}^2 [\psi_{1,k,-}]^2 [\psi_{L,k,-}]^2}{(\gamma^2 + \epsilon_k^2) ([\psi_{1,k,-}]^2 + [\psi_{L,k,-}]^2)} \right\}, \quad (33)$$

with $\mathcal{J} = \min\{J_e, J_o\}$. At a value of k corresponding to a localized state, at large enough system length L , either $\psi_{L,k,-}^2$ is exponentially suppressed compared to $\psi_{1,k,-}^2$ or vice versa, thus resulting in an overall suppression of the corresponding contribution to I_{NESS} . At variance, within the window of

delocalized states we obtain $[\psi_{1,k,-}]^2 [\psi_{L,k,-}]^2 / ([\psi_{1,k,-}]^2 + [\psi_{L,k,-}]^2) \approx (2L)^{-1}$. Neglecting also the dependence of the group velocity $v_k = \partial_k \epsilon_k$ on k (which is appropriate far enough from the band edge), we eventually obtain

$$I_{\text{NESS}} \approx \frac{2g^2 \mathcal{J}^2}{\pi} \arctan \left[\frac{\alpha \sqrt{L}}{\gamma} \right], \quad (34)$$

with α being a constant. The right-hand side of Eq. (34) takes a finite limit as $L \rightarrow \infty$. Clearly, an expression like Eq. (34) is strictly related to the presence of a mobility edge within the allowed band of states, without which one would again obtain a complete, localization induced, exponential suppression of I_{NESS} as a function of L .

Along the derivation we performed in the case of bond disorder, we again employed LE approach to compute I_{NESS} in the large-bias limit in the presence of dimer disorder of strength W [see Eq. (4)], as a function of W/J and of Δ , for increasing values of L and with $\Delta = \frac{\delta J}{J}$ where $J = \frac{J_e + J_o}{2}$ and $\delta J = \frac{J_e - J_o}{2}$. Again, to account for the effects of the disorder, at each value of W/J and Δ we ensemble averaged I_{NESS} over $N = 50$ realizations of the dimer disorder, with probability of having a single altered dimer set at $1 - \sigma = 0.5$. As in Fig. 3, we have chosen $\Gamma_1 = \gamma_L \equiv \gamma = 2$. Aside from the trivial line $W = 0$, we can clearly identify the light-green/light-blue regions at finite W/J with the set of delocalized states around the mobility edge. Taking into account that, in Fig. 5 we are choosing our energy units so $J_e = 1 + \Delta$ and $J_o = 1 - \Delta$, we see that the light-colored region is stuck at the line $W/J = 2J_o/J = (2 - 2\Delta)/J$. As expected, on increasing L there is a mild sharpening of the light-colored regions, simply related to the corresponding reduction of the width of the region of extended states. Yet, the peak value of I_{NESS} is not suppressed as L gets large, thus fully confirming the persistence of the mobility edge in that limit.

As a cross-check of our conclusions, in Fig. 6 we show a sample of the scaling of I_{NESS} with L at a specific point of the diagram in Fig. 5. Specifically, we draw I_{NESS} as a function of L for $20 \leq L \leq 160$ for $\Delta = -0.4$ and for $W/J = 0.1$ (blue curve), $W/J = 0.2$ (green curve), and $W/J = 2.6$ (red curve), by taking the system to the large bias limit, with the couplings between the chain and the bath chosen as in Fig. 5. At both points at $W/J = 0.1$ and $W/J = 2.6$ (that is, close to the mobility edge), we see practically no scaling of the current with the system size, which is consistent with the conclusion, evidenced by Fig. 5, that at both points the chain is in the conducting phase. At variance, as soon as we move off the mobility edge, we see a suppression of I_{NESS} as L increases, which is evident already at $W/J = 0.2$.

To conclude, we have shown how, connecting the disordered SSH chain to two baths in the large bias limit and probing the steady-state current in the NESS that sets in, provides an effective mean to map out the insulating and the conducting phases of the system, as well as the localization-delocalization phase transitions between them. In particular, we have evidenced how the value of I_{NESS} is strongly sensitive to the evolution of the system through the mobility edge that arises in the presence of correlated dimer disorder. To complement the results of this section, in the following

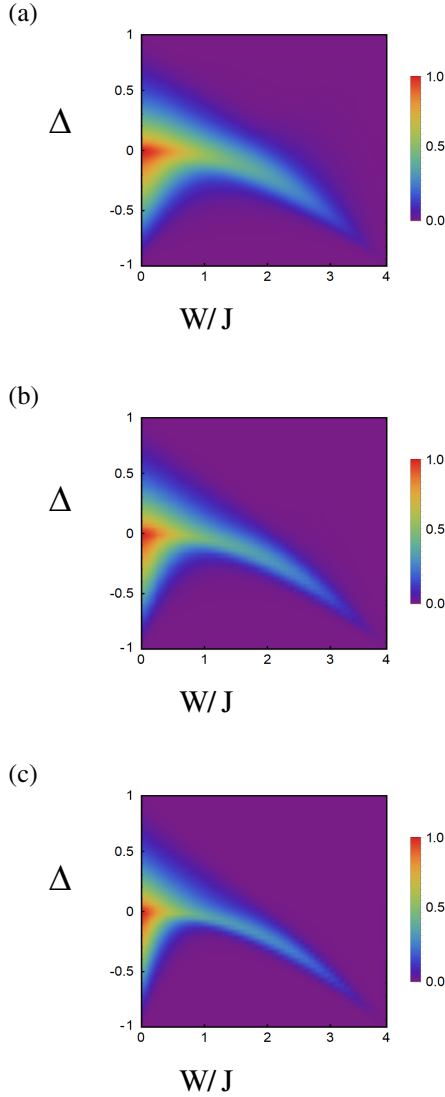


FIG. 5. (a) I_{NESS} in an $L = 20$ SSH chain with dimer disorder i with $\sigma = 0.5$ [see Eq. (4)], as a function of W/J and of Δ , with $J = \frac{J_e + J_o}{2}$ and $\Delta = \frac{J_e - J_o}{2}$ and for $0 \leq W/J \leq 4$ and for $-1 \leq \Delta \leq 1$. The figure has been generated by averaging over $N = 50$ different realizations of the dimer disorder. The couplings to the Lindblad baths have been set so $\Gamma_1 = \gamma_L = \gamma = 2$. The color code highlights the value of I_{NESS} (normalized at its maximum) as evidenced in the figure. (b) Same as in (a) but with $L = 40$. (c) Same as in (a) but with $L = 80$.

we introduce the EOD occupation as a mean to map out the disorder-induced topological phase transitions in the system.

IV. THE EVEN-ODD DIFFERENTIAL OCCUPATION

We now introduce the EOD \bar{v} as a collective property of the NESS of the chain and show how it can be used to detect the topological/trivial nature of the NESS.

When the system is at equilibrium, the onset of the topological phase corresponds to a nonzero value of the winding number w [79]. Alternative physical quantities sensible to the onset of nontrivial topology have been proposed, such as the charge polarization [7,79], and the dielectric polarization [80].

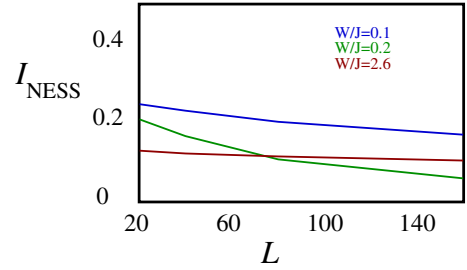


FIG. 6. I_{NESS} as a function of L for $20 \leq L \leq 160$ computed in a SSH chain with $J_e = 1 + \Delta$, $J_o = 1 - \Delta$, $\Delta = -0.4$, with couplings to the Lindblad baths set so that $\Gamma_1 = \gamma_L = \gamma = 2$, at a given realization of dimer disorder, with $W/J = 0.1$ (blue line), $W/J = 0.2$ (green line), +99 and $W/J = 2.6$ (red line).

Finally, the DAWN in Eq. (6) has been proposed in the presence of disorder described by a potential that anticommutes with Γ [21].

In the general case of a topological system in the presence of disorder, an effective mean to define the topological phase is by first ensemble-averaging over the disorder a quantity ν that is 0 in the trivial phase and $\neq 0$ (and quantized) in the topological phase and then by defining a threshold value of ν above which the system is assumed to be in the topological phase [15].

To introduce the EOD and to illustrate its meaning, let us focus, for the time being, on an L -site (with L even) SSH chain at equilibrium, in the extreme limits. These are defined by, respectively, sending $J_e \rightarrow 0$ while keeping J_o finite (the trivial extreme state) and by sending $J_o \rightarrow 0$ by keeping J_e finite (the topological extreme state). Denoting with $H_{\text{ext,Tr}}$ and with $H_{\text{ext,To}}$ the Hamiltonian of the system, respectively, describing the trivial and the topological extreme state, we obtain

$$H_{\text{ext,Tr}} = -J_o \sum_{r=1}^{\frac{L}{2}} \{c_{2r-1}^\dagger c_{2r} + c_{2r}^\dagger c_{2r-1}\},$$

$$H_{\text{ext,To}} = -J_e \sum_{r=1}^{\frac{L}{2}-1} \{c_{2r}^\dagger c_{2r+1} + c_{2r+1}^\dagger c_{2r}\}. \quad (35)$$

To diagonalize the Hamiltonians in Eqs. (35), we rewrite them as

$$H_{\text{ext,Tr}} = J_o \sum_{r=1}^{\frac{L}{2}} \{d_{r,u}^\dagger d_{r,u} - d_{r,g}^\dagger d_{r,g}\},$$

$$H_{\text{ext,To}} = J_e \sum_{r=1}^{\frac{L}{2}-1} \{f_{r,u}^\dagger f_{r,u} - f_{r,g}^\dagger f_{r,g}\}, \quad (36)$$

with, respectively,

$$d_{r,g} = \frac{c_{2r-1} + c_{2r}}{\sqrt{2}}, \quad d_{r,u} = \frac{c_{2r-1} - c_{2r}}{\sqrt{2}},$$

$$f_{r,g} = \frac{c_{2r} + c_{2r+1}}{\sqrt{2}}, \quad f_{r,u} = \frac{c_{2r} - c_{2r+1}}{\sqrt{2}}. \quad (37)$$

Defining the empty state $|0\rangle$ so $c_j|0\rangle = 0, \forall j = 1, \dots, L$, from Eqs. (36) and (37) we readily see that, in the trivial

extreme limit, the ground state $|\text{Tr}\rangle$ is uniquely given by

$$|\text{Tr}\rangle = \prod_{r=1}^{\frac{L}{2}} d_{r,g}^\dagger |\mathbf{0}\rangle. \quad (38)$$

At variance, in the topological extreme limit, the ground state is twofold degenerate: In this case, two orthogonal ground states $|L, \text{To}\rangle$ and $|R, \text{To}\rangle$ are given by

$$|L, \text{To}\rangle = c_1^\dagger \prod_{r=1}^{\frac{L}{2}-1} f_{r,g}^\dagger |\mathbf{0}\rangle, \quad |R, \text{To}\rangle = c_L^\dagger \prod_{r=1}^{\frac{L}{2}-1} f_{r,g}^\dagger |\mathbf{0}\rangle. \quad (39)$$

The two states in Eq. (39) correspond to the zero-energy Dirac fermion localized at either endpoint of the chain [23,81]. It is worth stressing that this is drastically different from what happens with the superconducting Kitaev chain, where a zero-energy Dirac fermion can only be built as a superposition of the two Majorana modes at the endpoints of the chain (and is, therefore, nonlocal in real space).

To discriminate between the states in Eqs. (38) and (39), we define the EOD \bar{v} as the average of the operator Γ in Eq. (5), that is, $\bar{v} = \text{Tr}[\Gamma\rho]$. Basically, \bar{v} measures the net average occupancy of the odd sites minus the one of the even sites of the chain.

At equilibrium, when $T = 0$, \bar{v} reduces to the ground-state average of Γ . In the extreme limits discussed above, $|\text{Tr}\rangle$, $|L, \text{To}\rangle$, and $|R, \text{To}\rangle$ are all eigenstates of Γ with eigenvalues respectively equal to 0, 1, and -1 . In general, when computing a thermodynamical average using the density matrix, we expect that, being degenerate in energy, $|L, \text{To}\rangle$ and $|R, \text{To}\rangle$ equally weight for the final result, thus eventually implying $\bar{v} = 0$. Therefore, to have a nonzero \bar{v} , we have to favor one of the two states with respect to the other. As we are going to argue in the following, connecting the chain to two Lindblad baths in the large-bias limit does perfectly accomplish this task.

To motivate our choice, in Fig. 7, we draw the real space density n_j over an $L = 20$ SSH chain connected to Lindblad baths, computed, respectively, for $J_e = 1.5, J_o = 1$ [Fig. 7(a), corresponding to the topological phase], for $J_e = J_o = 1$ [Fig. 7(b), corresponding to the topological phase transition], and for $J_e = 0.5, J_o = 1$ [Fig. 7(c), corresponding to the topologically trivial phase]. In all three cases, we have considered the chain without disorder and in the large bias limit, with $\Gamma_1 = \gamma_L = 2$ (in units of J_o). Figure 7(b) is a particular case of the density distribution in a one-dimensional conducting chain at half filling connected to two Lindblad baths in the large bias limit [60]. The density is uniform and constantly equal to $1/2$ everywhere, except at the two end sites of the chain, where, due to the coupling to the baths, the density is shifted upward or downward from the otherwise uniform value. n_j as a function of j shows a similar trend in Figs. 7(a) and 7(c), except that now there is a staggering that modulates the decay from the boundary values to the uniform bulk value $1/2$. In the topological case [Fig. 7(a)], the first and second oscillations, starting from either endpoint and moving toward the bulk of the chain, are large and in opposite directions: this makes $n_1 - n_2$ and $n_{L-1} - n_L$ provide by large the leading contribution to \bar{v} . In addition, $n_2 - n_3$ ($n_{L-2} - n_{L-1}$) have opposite signs with respect to $n_1 - n_2$ ($n_{L-1} - n_L$): All

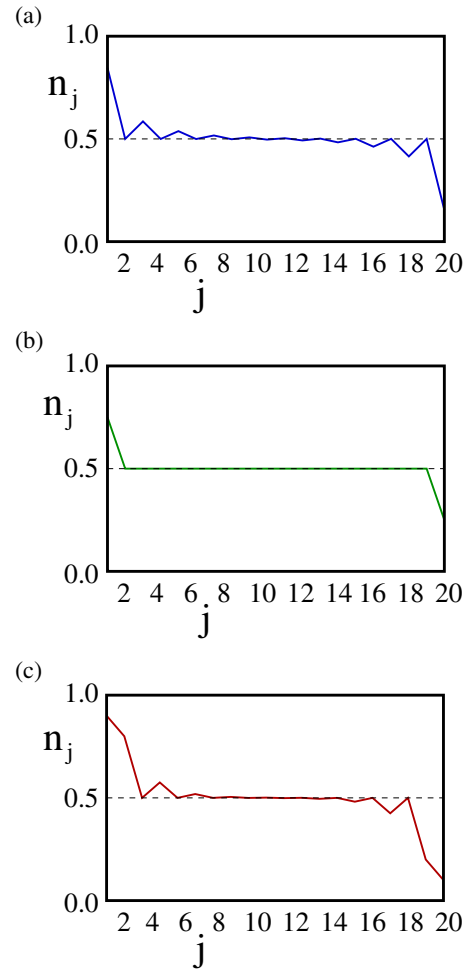


FIG. 7. (a) n_j as a function of j in an $L = 20$ SSH chain with $J_e = 1.5$ and $J_o = 1$, connected to two baths in the large bias limit, with $\Gamma_1 = \gamma_L = 2$. (b) n_j as a function of j in an $L = 20$ SSH chain with $J_e = 1$ and $J_o = 1$, connected to two baths in the large bias limit, with $\Gamma_1 = \gamma_L = 2$. (c) n_j as a function of j in an $L = 20$ SSH chain with $J_e = 0.5$ and $J_o = 1$, connected to two baths in the large bias limit, with $\Gamma_1 = \gamma_L = 2$.

this is expected to make the EOD large and pretty close to either $+1$ or -1 , depending on the sign of the bias between the baths. At variance, in the trivial case [Fig. 7(c)] $n_1 - n_2$ and $n_2 - n_3$, as well as $n_{L-2} - n_{L-1}$ and $n_{L-1} - n_L$, are apparently smaller than in the topological case and, more importantly, they have the same sign, being comparable in size, as well. This is now expected to make the EOD small, and close to 0.

To double check our conclusion, we now connect an SSH chain with $L = 20$ sites to two baths by its endpoints and set the parameters in Eqs. (9) so $\Gamma_1 = \gamma_L = \frac{g}{2}(1-f)$, $\gamma_1 = \Gamma_L = \frac{g}{2}(1+f)$, with $g = 2$ and $-1 \leq f \leq 1$ (so the large-bias limits correspond to either $f = 0$ or to $f = 1$). In Fig. 8, we plot a sample of our results: In particular, in both panels of the figure we draw the critical sweep, done by computing \bar{v} at $J_e = J_o = 1.0$ and by varying f , as well as a sweep realized in the topological region [$J_e = 1.2, J_o = 1.0$ in Fig. 8(a), $J_e = 1.5, J_o = 1.0$ in Fig. 8(b)] and another one realized in the trivial region [$J_e = 0.8, J_o = 1.0$ in Fig. 8(a), $J_e = 0.5, J_o = 1.0$ in Fig. 8(b)]. Apparently, moving from the trivial to the

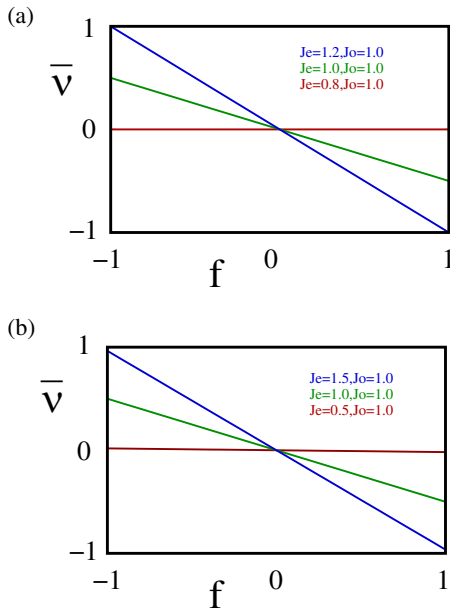


FIG. 8. (a) \bar{v} as a function of f in an SSH chain with $L = 20$ sites connected to two Lindblad baths characterized by $\Gamma_1 = \gamma_L = \frac{g}{2}(1 - f)$, $\gamma_1 = \Gamma_L = \frac{g}{2}(1 + f)$ [see Eq. (9) and the corresponding discussion for details] with $g = 2$ and $-1 \leq f \leq 1$, with $J_e = 1.2, J_o = 1.0$ (blue line), $J_e = J_o = 1.0$ (green line), $J_e = 0.8, J_o = 1.0$ (red line). (b) Same as in (a), but with $J_e = 1.5, J_o = 1.0$ (blue line), $J_e = J_o = 1.0$ (green line), $J_e = 0.5, J_o = 1.0$ (red line).

topological region determines an increase in \bar{v} by at least two orders of magnitude. In addition, in the large-bias limit and in the topological region, \bar{v} converges to the universal value ± 1 , depending on the sign of the bias.

As a complementary analysis, we have also computed \bar{v} in the large bias limit across the topological phase transition for different values of the system length L . In Fig. 9, we plot our results for \bar{v} as a function of J_e/J_o , with J_o held fixed at 1, $\Gamma_1 = \gamma_L = g = 2$, $\gamma_1 = \Gamma_L = 0$, and $-0.5 \leq J_e \leq 1.5$, for $L = 20$ (red curve), $L = 40$ (green curve), and $L = 80$ (blue curve). We evidence the apparent switch of \bar{v} from the value ~ 0 that it takes within the trivial region to the value ~ 1 that it takes in the large bias limit within the topological region. In addition,

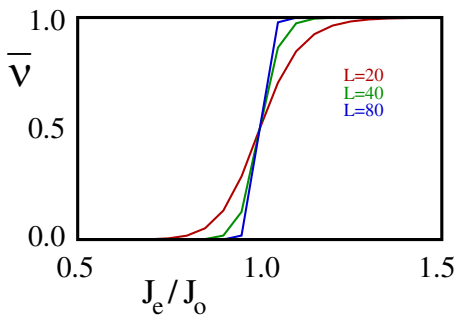


FIG. 9. \bar{v} as a function of f in an SSH chain connected to two Lindblad baths in the large bias limit ($\Gamma_1 = \gamma_L = g = 2$, $\gamma_1 = \Gamma_L = 0$) as a function of J_e/J_o for $0.5 \leq J_e/J_o \leq 1.5$, with the length of the chain $L = 20$ (red curve), $L = 40$ (green curve), and $L = 80$ (blue curve).

we appreciate how, the larger L is, the sharper the crossover region between the two limiting values, thus suggesting that, for large enough L , \bar{v} just switches between 0 and 1 (or vice versa) at the topological phase transition.

Of course, all our results of this section apply to the clean limit. We now discuss how they are affected by the presence of disorder.

A. The even-odd differential occupation at nonzero bond disorder

By construction, any realization of the bond disorder potential anticommutes with Γ . This implies that all the nondegenerate states of the disordered Hamiltonian at fixed disorder are grouped in pairs with opposite energies, with states in a pair connected to each other by Γ . Thus, we expect that when pushing the chain to the large bias limit and probing \bar{v} at a given realization of the disorder, either the system is in the topologically trivial phase and $\bar{v} = 0$ or it is in the nontrivial phase and, in the large-bias limit, we obtain $\bar{v} = \pm 1$ (depending on the sign of the applied bias): The relative probability of the two results is a function of only the disorder strength. Counting how many times, over several realizations of the disorder, $|\bar{v}| = 1$, evidences whether the disorder itself is strong enough to destroy the topological phase or not.

Here we first verify that, at a single realization of the disorder with variable disorder strength W , \bar{v} is either ± 1 , or 0, depending on whether the model with the effective J_o renormalized by the disorder lies within the topological or the trivial phase. We consider an $L = 40$ site chain connected to two external baths in the large bias limit, with $\Gamma_1 = \gamma_L = 2$ and $\gamma_1 = \Gamma_L = 0$. The disorder is described by the distribution in Eq. (3), with varying W . In Fig. 10(a), we show a color plot of the measured EOD as a function of both W/J_o and J_e/J_o , with J_o normalized to 1, used as the reference energy scale. The red area corresponds to $\bar{v} = 1$, the deep purple area to $\bar{v} = 0$. In Figs. 10(b) and 10(c), we show a scatter plot of the energy levels of the chain as a function of W/J_o at J_e/J_o fixed and equal to 1.5 and to 0.5, so, in the clean limit, the chain lies within, respectively, the topological, and the trivial phases. We evidence with a red arrow the emerging in-gap states in both cases, which are the fingerprint of a topologically nontrivial system. We clearly see that the red (deep purple) region of Fig. 10(a) corresponds to regions with a pair of in-gap states (no in-gap states) in the level diagram of the system, thus supporting the effectiveness of using the EOD as a tool to monitor the onset of the topological phase.

To check the sharpening of the transition on increasing the chain length L , we have computed \bar{v} in a disordered chain in the large bias limit with $\Gamma_1 = \gamma_L = 2$ and $\gamma_1 = \Gamma_L = 0$, by ensemble averaging over $N = 50$ realizations of the bond disorder extracted using $\mathcal{P}_b[J_o]$ in Eq. (3) at increasing L , for $L = 20$, $L = 40$, and $L = 80$. We present the corresponding result in Fig. 11 by using the same style as in Fig. 10(a) but, of course, by now reporting the ensemble-averaged results. The sharpening of the (light colored) transition region is apparent, which enforces our interpretation of the nature of the phase transition.

Having shown the effectiveness of the EOD in monitoring the onset of the topological phase in the disordered system

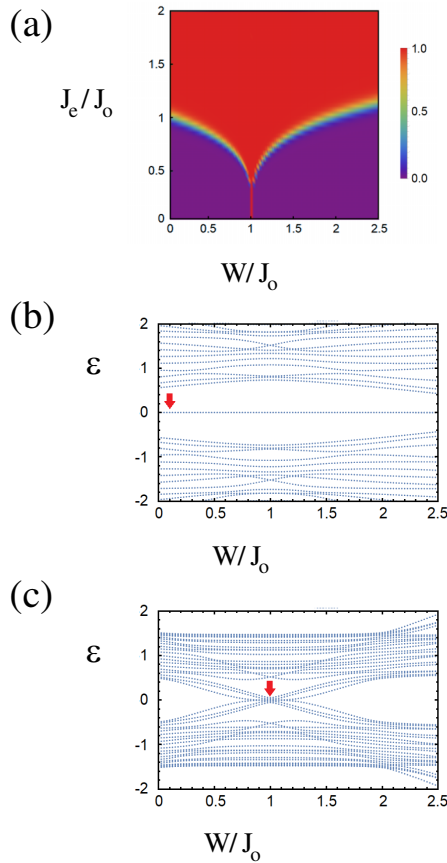


FIG. 10. (a) $\bar{\nu}$ computed in an SSH chain with $L = 40$ in the large bias limit with $\Gamma_1 = \gamma_L = 2$ and $\gamma_1 = \Gamma_L = 0$, at a single configuration of bond disorder as a function of W/J_0 and of J_e/J_0 , with J_0 (in the clean limit) used as the reference energy scale for the system. Red regions correspond to $\bar{\nu} = \pm 1$, deep purple regions to $\bar{\nu} = 0$. (b) Energy levels of the chain as a function of W/J_0 at $J_e/J_0 = 1.5$ (the in-gap states are evidenced by the red arrow). (c) Same as in (b) but with $J_e/J_0 = 0.5$.

taken at large bias with bond disorder, we now repeat the same analysis in the case in which the disorder is realized with a random distribution of dimer impurities.

B. The even-odd differential occupation at nonzero dimer disorder

Differently from alternative means, such as the DAWN, which does not work if the disorder does not anticommute with Γ [21,65], as we show next, the EOD also works with the (nonchiral) dimer disorder.

First, let us note that since the disorder potential no longer anticommutes with Γ , we no longer expect (in the large- L limit) a sharp borderline between the region with $\bar{\nu} = \pm 1$ and the region with $\bar{\nu} = 0$. This is apparent in Fig. 12(a), where we plot $\bar{\nu}$ computed in an SSH chain with $L = 40$ at a single realization of the dimer disorder, as a function of the disorder strength normalized to the average hopping W/J , with $J = \frac{J_e + J_0}{2}$, and of $\Delta = \frac{\delta J}{J}$ with $\delta J = \frac{J_e - J_0}{2}$. From Fig. 12(a), we see that, on increasing W at fixed $\Delta (> 0)$ (that is, starting from the topological phase, in the clean limit), the EOD smoothly evolves from the red region at small disorder

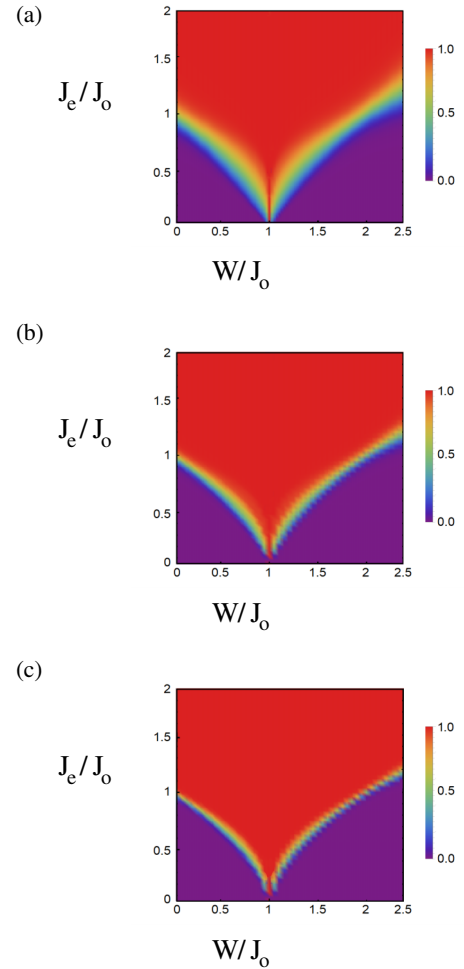


FIG. 11. (a) $\bar{\nu}$ computed in an SSH chain with $L = 20$ in the large bias limit $\Gamma_1 = \gamma_L = 2$ and $\gamma_1 = \Gamma_L = 0$, and with chiral disorder by averaging over 50 realizations of the disorder by varying W/J_0 and J_e/J_0 . (b) Same as in (a) but with $L = 40$. (c) Same as in (a) but with $L = 80$.

(with $\bar{\nu} = \pm 1$) to a yellow, then green, then light blue region, corresponding to progressively (and continuously) decreasing values of $|\bar{\nu}|$. To relate this behavior to a possible suppression of the topological phase, we again consider the energy levels at the same realization of the disorder as a function of W/J . An important point here is that, since, differently from the bond disorder, introducing dimer impurities does alter the overall chemical potential, to have a common energy reference at any value of W/J we systematically subtract from the computed energy eigenvalues the extra overall chemical potential determined by the added impurity (impurities). Doing so, we obtain the plots in Figs. 12(b)–12(e), where we draw the energy levels as a function of W/J at a single realization of the disorder and for, respectively, $\Delta J = -0.25, 0.25, 0.50, 0.95$. In Figs. 12(c)–12(e), we highlight with a red arrow the pair of in-gap states that are the fingerprint of the topological phase, to which the system goes back as $W \rightarrow 0$. Of course, we see no in-gap states in Fig. 12(b), as, in this case, the system goes to the trivial phase as $W \rightarrow 0$. It is worth stressing that, due to the peculiar nature of dimer disorder, increasing W moves the in-gap states toward either the upper or the lower gap

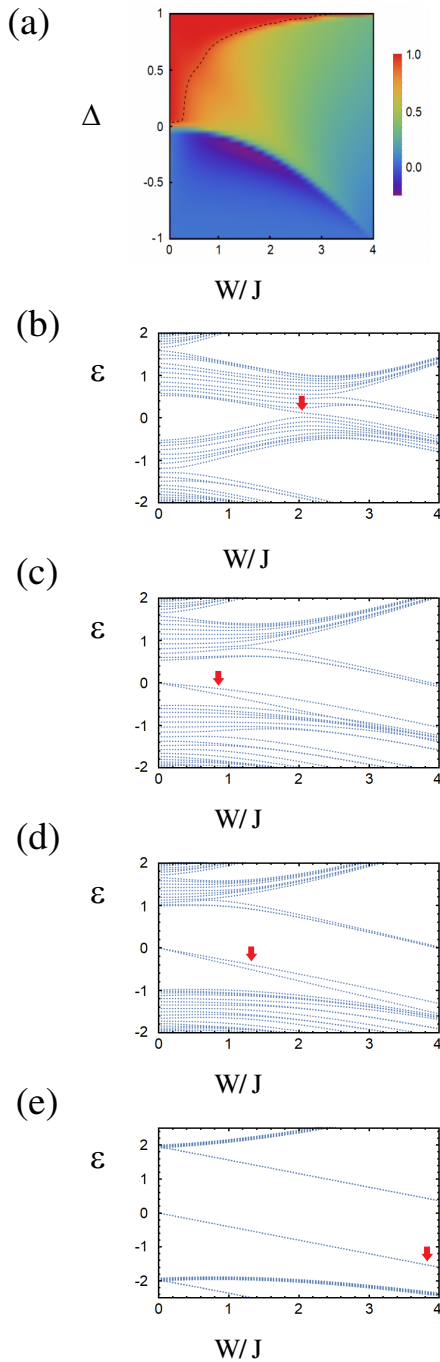


FIG. 12. (a) $\bar{\nu}$ computed in an SSH chain with $L = 40$ in the large bias limit with $\Gamma_1 = \gamma_L = 2$ and $\gamma_1 = \Gamma_L = 0$ at a single configuration of dimer disorder as a function of W/J and of $\Delta = \frac{J_e - J_o}{J_e + J_o}$. Red regions correspond to $\bar{\nu} = \pm 1$. The dashed black line marks the points at which $\bar{\nu} = \bar{\nu}_* = 0.90$. (b) Energy levels of the chain as a function of W/J at $\Delta = -0.25$. (c) Same as in (b) but with $\Delta = 0.25$ (now the in-gap states are evidenced by a red arrow). (d) Same as in (c) but with $\Delta = 0.50$. (e) Same as in (c) but with $\Delta = 0.95$.

edge (depending on the sign of W). Over a finite- L disordered chain, it is therefore natural to assume that the in-gap states merge with the other states when their energy, measured with respect to the closer gap edge, equates the average spacing between the other states. Using this criterion, we see that,

on increasing W , the in-gap doublet merges with the other states at a value of the disorder strength which, by looking at the color plot in Fig. 12(a), we realize corresponds to a color crossover from red to yellow-green. On the numerical side, this means that $\bar{\nu}$ become < 1 at the point in which the in-gap states merge with the other states and the topological phase is lost. Accordingly, we can use $\bar{\nu}$ to define a border for the topological phase as the line at which the EOD takes a conventional value, which we choose to be $\bar{\nu}_* = 0.90$ (other choices such as, for instance, $\bar{\nu}_* = 0.85$ do not substantially affect the shape of the borderline). In Fig. 12(a), we draw as a dashed black line the borderline of the topological phase that we define in this way.

To infer if, and to what extent, increasing the system size L affects the global behavior of the EOD as a function of W/J and of Δ (and, therefore, the shape and the position of the borderline of the topological phase), we have computed $\bar{\nu}$ by ensemble averaging over $N = 50$ realizations of the dimer disorder in an SSH chain taken to the large bias limit with $\Gamma_1 = \gamma_L = 2$ and $\gamma_1 = \Gamma_L = 0$, by varying both W/J and Δ and for $L = 20, 40$, and 80 . We draw the corresponding diagrams in Fig. 13: By comparing the plots in Figs. 13(a)–13(c) (corresponding to $L = 20, 40, 80$) with each other, we see no appreciable difference in the behavior of $\bar{\nu}$ in the topological region. Thus, on one hand we conclude that the dimer disorder tends to suppress the topological phase of the SSH chain, except for a region originating from the line $W = 0, 0 < \Delta$ and extending toward the right. On the other hand, the border of such a region, which we conventionally attributed to $\nu = \nu_* = 0.90$, is not substantially affected by increasing L : Contrary to what happens with bond disorder, with dimer disorder there is no sharpening of the transition on increasing L .

To conclude, we evidence how, despite the apparent difficulty of even defining the borderline of the topological region in the presence of dimer disorder, taking the (open) chain in the large bias limit and going through a synoptic comparison of the variation of the EOD $\bar{\nu}$ as a function of the system parameters and of the evolution of the system levels as a function of the disorder strength at fixed Δ allows us to mark the border of the topological region even in this case.

Combining the results of the EOD and of I_{NESS} for both kinds of disorder we have discussed above allows for mapping out the complete phase diagram of the SSH chain connected to two Lindblad reservoirs in the large bias limit as a function of the chain parameters as well as of the strength of the disorder.

V. CONCLUSIONS

We have applied the LE method to derive the phase diagram of an open SSH chain connected to two external baths in the large bias limit, in the presence of bond and of dimer disorder. Biasing the external baths has allowed us to stabilize a NESS, characterized by a steady current I_{NESS} . Whether I_{NESS} flows to 0, or to a finite value, in the limit of large chain length L , tells us whether the system is fully localized by disorder or not.

Our approach just needs a simple transport measurement, combined with an appropriate scaling analysis, to map out the localization/delocalization transition in the disordered chain.

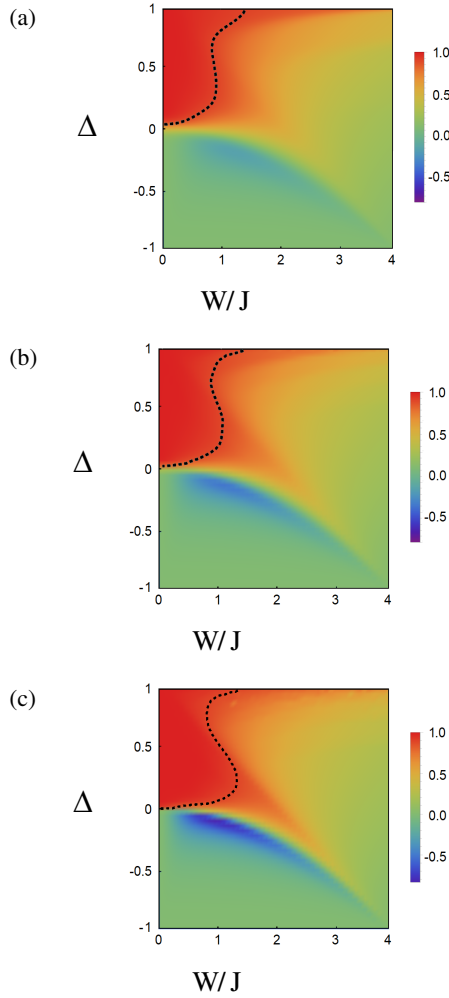


FIG. 13. (a) \bar{v} computed in an SSH chain with $L = 20$ in the large bias limit with $\Gamma_1 = \gamma_L = 2$ and $\gamma_1 = \Gamma_L = 0$, in the presence of dimer disorder by averaging over 50 realizations of the disorder by varying W/J and Δ . As in Fig. 12, the dashed black line marks the points at which $\bar{v} = 0.90$. (b) Same as in (a) but with $L = 40$. (c) Same as in (a) but with $L = 80$.

In particular, our method has proven to be effective in evidencing the expected onset of the mobility edge which, in the case of dimer disorder, marks the opening of the window of delocalized states in the otherwise fully localized band [19,64,69].

We have used the (ensemble averaged) EOD occupancy to distinguish between topologically trivial and nontrivial phases. From the presence of in-gap states, in the spectrum of the SSH chain at a given realization of disorder, we have been able to relate a nontrivial topological phase to an average EOD $\bar{v} = \pm 1$ (depending on the sign of the applied bias). Computing the EOD poses no constraints on the symmetries of the disorder potential: as we show, we can compute the EOD regardless of whether the disorder anticommutes with Γ or not. Thus, using the EOD, we can circumvent the limitations of alternative quantity, such as the DAWN [21,65].

Of course, a meaningful definition and implementation of the EOD requires that the system is taken to the out-of-equilibrium regime into an appropriate NESS. We therefore conclude that, by driving the disordered SSH chain toward the

large bias regime and by performing the appropriate measurements on the NESS that sets in, it is possible to map out the complete phase diagram of the system, both for what concerns the localization/delocalization phase transition, as well as the topological phase transition, in the presence of disorder.

While, to define and illustrate the application of our method, in this paper we limited ourselves to a well-known and widely discussed physical system, such as the disordered SSH chain, there are no particular limitations in extending our technique to more complex and/or less investigated models. In this direction, an intriguing perspective we intend to pursue is applying our method to a disordered SSH chain with long-range single-electron hopping and/or interaction. In this case, a derivation of I_{NESS} as a function of the system parameters should allow for probing the emergence of mobility edge(s) in the system, as a consequence of the long-range nature of the correlations [82]. Moreover, monitoring \bar{v} should provide us with detailed information about the onset of unconventional topological phases, which are in general expected to emerge in systems with long-range correlations [83,84].

Other possible applications should concern, for instance, topological Kondo systems at junctions of quantum wires [85–92]. Finally, as an additional possible development of our work, we believe it is worth mentioning the use of a multisite Lindblad bath to attempt to smoothly interpolate between the linear response, Landauer-Büttiker like regime, and the large bias limit to connect the behavior of I_{NESS} to the current response of the system in the linear regime.

ACKNOWLEDGMENTS

A.N. and D.G acknowledge financial support from Italy's MIUR PRIN project TOP-SPIN (Grant No. PRIN 20177SL7HC).

APPENDIX A: DERIVATION OF EQ. (14)

In this Appendix, we illustrate the derivation of Eq. (14) of the main text for the matrix $\mathcal{C}(t)$ by focusing, as a specific example, on the equation for the matrix element $\mathcal{C}_{1,1}(t)$.

The starting point is the canonical anticommutation relations between the lattice single-fermion operators

$$\{c_i^\dagger, c_j\} = \delta_{i,j}, \quad \{c_i^\dagger, c_j^\dagger\} = \{c_i, c_j\} = 0. \quad (\text{A1})$$

By writing the system Hamiltonian H as $H = \sum_{i,j=1}^L c_i^\dagger \mathcal{H}_{i,j} c_j$ and by employing Eqs. (A1), we obtain (term by term)

$$\begin{aligned} (1) \quad \langle [H, c_1^\dagger c_1] \rangle &= \left\langle \left[\sum_{i,j=1}^L c_i^\dagger \mathcal{H}_{i,j} c_j, c_1^\dagger c_1 \right] \right\rangle \\ &= \sum_{j \neq 1} \mathcal{H}_{1,j} \langle [c_1^\dagger c_j, c_1^\dagger c_1] \rangle + \sum_{i \neq 1} \mathcal{H}_{i,1} \langle [c_i^\dagger c_1, c_1^\dagger c_1] \rangle \\ &= \sum_{j \neq 1} \mathcal{H}_{1,j} \langle -c_1^\dagger c_j \rangle + \sum_{i \neq 1} \mathcal{H}_{i,1} \langle c_i^\dagger c_1 \rangle \\ &= - \sum_j [\mathcal{H}_{1,j} \mathcal{C}_{1,j} - \mathcal{H}_{j,1} \mathcal{C}_{j,1}] = [\mathcal{H}^T, \mathcal{C}]_{1,1}, \end{aligned} \quad (\text{A2})$$

(2)

$$\begin{aligned} \Gamma_1 \langle c_1 c_1^\dagger c_1 c_1^\dagger \rangle &= \Gamma_1 \langle c_1 (1 - c_1 c_1^\dagger) c_1^\dagger \rangle = \Gamma_1 \langle c_1 c_1^\dagger \rangle \\ &= \Gamma_1 - \Gamma_1 \langle c_1^\dagger c_1 \rangle, \end{aligned} \quad (\text{A3})$$

(3)

$$-\frac{\Gamma_1}{2} \langle \{c_1 c_1^\dagger, c_1^\dagger c_1\} \rangle = -\frac{\Gamma_1}{2} \langle c_1 c_1^\dagger c_1^\dagger c_1 + c_1^\dagger c_1 c_1 c_1^\dagger \rangle = 0, \quad (\text{A4})$$

(4)

$$\begin{aligned} \Gamma_L \langle c_L c_1^\dagger c_1 c_L^\dagger \rangle - \frac{\Gamma_L}{2} \langle \{c_L c_L^\dagger, c_1^\dagger c_1\} \rangle \\ = \Gamma_L \langle c_1^\dagger c_1 c_L c_L^\dagger \rangle - \frac{\Gamma_L}{2} \langle c_1^\dagger c_1 c_L c_L^\dagger + c_1^\dagger c_1 c_L c_L^\dagger \rangle \\ = 0, \end{aligned} \quad (\text{A5})$$

(5)

$$\gamma_1 \langle c_1^\dagger c_1^\dagger c_1 c_1 \rangle = 0, \quad (\text{A6})$$

(6)

$$\begin{aligned} -\frac{\gamma_1}{2} \langle \{c_1^\dagger c_1, c_1^\dagger c_1\} \rangle &= -\frac{\gamma_1}{2} \langle c_1^\dagger c_1 c_1^\dagger c_1 + c_1^\dagger c_1 c_1^\dagger c_1 \rangle \\ &= -\gamma_1 \langle c_1^\dagger c_1 \rangle, \end{aligned} \quad (\text{A7})$$

(7)

$$\begin{aligned} \gamma_L \langle c_L^\dagger c_1^\dagger c_1 c_L \rangle - \frac{\gamma_L}{2} \langle \{c_L^\dagger c_L, c_1^\dagger c_1\} \rangle \\ = \gamma_L \langle c_L^\dagger c_L c_1^\dagger c_1 \rangle - \frac{\gamma_L}{2} \langle c_L^\dagger c_L c_1^\dagger c_1 + c_L^\dagger c_L c_1^\dagger c_1 \rangle \\ = 0. \end{aligned}$$

Adding the terms listed above all together, we obtain Eq. (14) of our paper for $\mathcal{C}_{1,1}(t)$. A straightforward generalization of the above procedure yields the equations for a generic matrix element $\mathcal{C}_{i,j}(t)$.

APPENDIX B: SOLUTION OF THE SSH MODEL IN THE CLEAN LIMIT

In this Appendix, we review the derivation of the single-particle wave functions for the SSH chain in the absence of disorder. In particular, we first solve the time-independent Schrödinger equation over an L -site open chain and derive the corresponding wave functions, which we used in Sec. III to analytically compute I_{NESS} . Then, we compute the scattering amplitudes across a single impurity, both in the case of a bond impurity and of a dimer impurity. The corresponding result for the reflection coefficient is what we used in Secs. III B and III C to analyze the impurity-induced localization in the NESS.

1. SSH chain with open boundary conditions

We now review the derivation of the eigenvalues and of the eigenfunctions of an L -site SSH chain with open boundary conditions. This is described by the Hamiltonian H_0 , given by

$$H_0 = - \sum_{j=1}^{L-1} J_{j,j+1} \{c_j^\dagger c_{j+1} + c_{j+1}^\dagger c_j\}, \quad (\text{B1})$$

with

$$J_{j,j+1} = \begin{cases} J_o & (j \text{ odd}) \\ J_e & (j \text{ even}), \end{cases} \quad (\text{B2})$$

supplemented with open boundary conditions at both the endpoints of the chain. Taking into account the staggering due to the term $\propto \delta J$, we consider energy eigenmodes in the form

$$\Gamma_\epsilon = \sum_{j=1}^L \{u_j + (-1)^j v_j\} c_j \equiv \sum_{j=1}^L \psi_j c_j, \quad (\text{B3})$$

with the open boundary conditions $u_{j=0} + v_{j=0} = u_{j=L+1} - v_{j=L+1} = 0$ (note that, as in the main text, here we are assuming that L is even). On imposing $[\Gamma_\epsilon, H_0] = \epsilon \Gamma_\epsilon$, we obtain the lattice, time-independent Schrödinger equation for the wave functions u_j, v_j in the form

$$\begin{aligned} \epsilon u_j &= -\frac{J_e + J_o}{2} \{u_{j+1} + u_{j-1}\} + \frac{J_e - J_o}{2} \{v_{j+1} - v_{j-1}\}, \\ \epsilon v_j &= -\frac{J_e - J_o}{2} \{u_{j+1} - u_{j-1}\} + \frac{J_e + J_o}{2} \{v_{j+1} + v_{j-1}\}, \end{aligned} \quad (\text{B4})$$

with $1 < j < L$. Assuming a solution of the form

$$\begin{bmatrix} u_j \\ v_j \end{bmatrix} = \begin{bmatrix} u_k \\ v_k \end{bmatrix} e^{ikj}, \quad (\text{B5})$$

with $-\frac{\pi}{2} \leq k \leq \frac{\pi}{2}$, we eventually trade Eq. (B4) for the analogous one in momentum space, given by

$$\begin{aligned} \epsilon u_k &= -(J_e + J_o) \cos(k) u_k + i(J_e - J_o) \sin(k) v_k, \\ \epsilon v_k &= -i(J_e - J_o) \sin(k) u_k + (J_e + J_o) \cos(k) v_k. \end{aligned} \quad (\text{B6})$$

The allowed values of ϵ are, therefore,

$$\pm \epsilon_k = \pm \sqrt{(J_e + J_o)^2 \cos^2(k) + (J_e - J_o)^2 \sin^2(k)}, \quad (\text{B7})$$

with the corresponding wave functions given by

$$\psi_{j,k,+} = c(-1)^j e^{(-1)^j \frac{i\varphi_k}{2}} e^{ikj}, \quad \psi_{j,k,-} = c e^{(-1)^j \frac{i\varphi_k}{2}} e^{ikj}. \quad (\text{B8})$$

In Eq. (B9) c is a normalization constant and

$$\cos(\varphi_k) = \frac{(J_e + J_o) \cos(k)}{\epsilon_k}, \quad \sin(\varphi_k) = \frac{(J_e - J_o) \sin(k)}{\epsilon_k}, \quad (\text{B9})$$

with $-\frac{\pi}{2} \leq k \leq \frac{\pi}{2}$. Due to the apparent degeneracy of the energy eigenvalues under $k \rightarrow -k$, we may combine degenerate solutions with opposite values of k to construct wave functions satisfying the open boundary conditions. These are given by

$$\begin{aligned} \psi_{j,k,+} &= (-1)^j \{ \alpha_{k,+} e^{(-1)^j \frac{i\varphi_k}{2}} e^{ikj} + \beta_{k,+} e^{(-1)^j \frac{i\varphi_k}{2}} e^{-ikj} \}, \\ \psi_{j,k,-} &= \{ \alpha_{k,-} e^{(-1)^j \frac{i\varphi_k}{2}} e^{ikj} + \beta_{k,-} e^{(-1)^j \frac{i\varphi_k}{2}} e^{-ikj} \}, \end{aligned} \quad (\text{B10})$$

with $\alpha_{k,\pm}, \beta_{k,\pm}$ constants to be determined by imposing open boundary conditions, that is,

$$\psi_{j=0,k,\pm} = \psi_{j=L+1,k,\pm}. \quad (\text{B11})$$

Equations (B10) and (B11) imply the secular equation for k given by

$$\sin[k(L+1) - \varphi_k] = 0. \quad (\text{B12})$$

Once k satisfies Eq. (B12), the solutions in Eq. (B10) take the form

$$\begin{aligned}\psi_{j,k,+} &= c(-1)^j \left\{ e^{[-(-1)^j-1]\frac{i\varphi_k}{2}} e^{ikj} - e^{-[(-1)^j-1]\frac{i\varphi_k}{2}} e^{-ikj} \right\}, \\ \psi_{j,k,-} &= c \left\{ e^{[-(-1)^j-1]\frac{i\varphi_k}{2}} e^{ikj} - e^{-[(-1)^j-1]\frac{i\varphi_k}{2}} e^{-ikj} \right\},\end{aligned}\quad (\text{B13})$$

with c being an overall normalization constant. In addition to the solutions discussed above, it is also possible to recover solutions with energy $|\epsilon| < 2|J_e - J_o|$. To derive them, we set $k = \frac{\pi}{2} - iq$. Accordingly, we obtain for the dispersion relation

$$\epsilon_q^2 = (J_e - J_o)^2 \cosh^2(q) - (J_e + J_o)^2 \sinh^2(q). \quad (\text{B14})$$

Equations (B6) now become

$$\begin{aligned}\epsilon u_q &= -i(J_e + J_o) \sinh(q) u_q + i(J_e - J_o) \cosh(q) v_q, \\ \epsilon v_q &= -i(J_e - J_o) \cosh(q) u_q + i(J_e + J_o) \sinh(q) u_q.\end{aligned}\quad (\text{B15})$$

Setting

$$e^{-i\varphi_\xi} = \left\{ \left(\frac{J_e + J_o}{J_e - J_o} \right) \tanh(q) - \frac{i\epsilon_q}{(J_e - J_o) \cosh(q)} \right\}, \quad (\text{B16})$$

we eventually find the real-space wave functions in the form

$$\begin{aligned}\psi_{j,0,+} &= \left\{ \alpha_{+,0} \left[i^j e^{\frac{i\varphi_\xi}{2}} + i^{-j} e^{-\frac{i\varphi_\xi}{2}} \right] e^{qj} \right. \\ &\quad \left. + \beta_{+,0} \left[i^j e^{-\frac{i\varphi_\xi}{2}} - i^{-j} e^{\frac{i\varphi_\xi}{2}} \right] e^{-qj} \right\}, \\ \psi_{j,0,-} &= \left\{ \alpha_{-,0} \left[i^j e^{-\frac{i\varphi_\xi}{2}} + i^{-j} e^{\frac{i\varphi_\xi}{2}} \right] e^{qj} \right. \\ &\quad \left. + \beta_{-,0} \left[-i^j e^{\frac{i\varphi_\xi}{2}} + i^{-j} e^{-\frac{i\varphi_\xi}{2}} \right] e^{-qj} \right\}.\end{aligned}\quad (\text{B17})$$

The allowed value of q is determined again by the secular equation, which is now given by

$$\tanh[q(L+1)] - \cos(\varphi_\xi) = 0. \quad (\text{B18})$$

Equation (B18) takes a real solution for q only if $J_e - J_o > 0$, which is the necessary condition to recover the topological phase. The wave functions for the in-gap modes obeying open boundary conditions are given by

$$\begin{aligned}\psi_{j,0,+} &= c \left\{ \sin\left(\frac{\varphi_\xi}{2}\right) \left[i^j e^{\frac{i\varphi_\xi}{2}} + i^{-j} e^{-\frac{i\varphi_\xi}{2}} \right] e^{qj} \right. \\ &\quad \left. + i \cos\left(\frac{\varphi_\xi}{2}\right) \left[i^j e^{-\frac{i\varphi_\xi}{2}} - i^{-j} e^{\frac{i\varphi_\xi}{2}} \right] e^{-qj} \right\}, \\ \psi_{j,0,-} &= c \left\{ \sin\left(\frac{\varphi_\xi}{2}\right) \left[i^j e^{-\frac{i\varphi_\xi}{2}} + i^{-j} e^{\frac{i\varphi_\xi}{2}} \right] e^{qj} \right. \\ &\quad \left. + i \cos\left(\frac{\varphi_\xi}{2}\right) \left[-i^j e^{\frac{i\varphi_\xi}{2}} + i^{-j} e^{-\frac{i\varphi_\xi}{2}} \right] e^{-qj} \right\}.\end{aligned}\quad (\text{B19})$$

The results presented in this Appendix are what we have used in the main paper to compute quantities concerning the SSH chain at equilibrium.

2. Scattering amplitudes in the presence of an impurity

We now derive the scattering amplitudes in a nonuniform chain, in the presence of either a bond or dimer impurity. Let us begin by considering a single bond impurity: this is defined by modifying the strength of a single odd bond from $J_o \rightarrow J_o + \delta J$. Focusing, for the time being, on the solution $\psi_{j,k,+}$ and without considering specific boundary conditions, we construct a scattering solution with momentum k incoming

from the left-hand side in the presence of a bond impurity. Assuming that the impurity is located across sites $j = 1$ and $j = 2$ and, correspondingly, alleging for a possible discontinuity of $\psi_{j,k,+}$ across the impurity, we set

$$\psi_{j,k,+} = \begin{cases} \psi_{j,k,+}^<, & (\text{for } j \leq 1) \\ \psi_{j,k,+}^>, & (\text{for } j \geq 2), \end{cases} \quad (\text{B20})$$

with $\psi_{j,k,+}^{<(>)} = c\{u_{j,k,+}^{<(>)} + (-1)^j v_{j,k,+}^{<(>)}\}$, c being a normalization constant, and

$$\begin{aligned}u_{j,k,+}^< &= (-1)^j i \sin\left(\frac{\varphi_k}{2}\right) \{e^{ikj} - r_k e^{-ikj}\}, \\ u_{j,k,+}^> &= (-1)^j i \sin\left(\frac{\varphi_k}{2}\right) t_k e^{ikj}, \\ v_{j,k,+}^< &= (-1)^j \cos\left(\frac{\varphi_k}{2}\right) \{e^{ikj} + r_k e^{-ikj}\}, \\ v_{j,k,+}^> &= (-1)^j \cos\left(\frac{\varphi_k}{2}\right) t_k e^{ikj},\end{aligned}\quad (\text{B21})$$

with r_k, t_k being the scattering amplitudes. The interface conditions across the impurities are given by

$$\begin{aligned}-(J_o + \delta J)\psi_{2,k,+}^> + J_o\psi_{2,k,+}^< &= 0, \\ J_o\psi_{1,k,+}^> - (J_o + \delta J)\psi_{1,k,+}^< &= 0.\end{aligned}\quad (\text{B22})$$

Inserting Eqs. (B21) into Eqs. (B22), we recover the system for the scattering amplitudes in the form

$$\begin{aligned}-(J_o + \delta J)e^{2ik+\frac{i\varphi_k}{2}} t_k + J_o \{e^{2ik+\frac{i\varphi_k}{2}} + r_k e^{-2ik-\frac{i\varphi_k}{2}}\} &= 0, \\ J_o e^{ik-\frac{i\varphi_k}{2}} t_k - (J_o + \delta J) \{e^{ik-\frac{i\varphi_k}{2}} + r_k e^{-ik+\frac{i\varphi_k}{2}}\} &= 0.\end{aligned}\quad (\text{B23})$$

Finally, from Eq. (B23) we obtain

$$r_k = -\frac{e^{4ik+i\varphi_k} \delta J (2J_o + \delta J)}{-J_o^2 + e^{2i(k+\varphi_k)} (J_o + \delta J)^2}. \quad (\text{B24})$$

In terms of the parameter W introduced in Eq. (3) and setting $J_o = 1$, we reexpress Eq. (B24) as

$$r_k = \frac{e^{4ik+i\varphi_k} W (2 - W)}{-1 + e^{2i(k+\varphi_k)} (1 - W)^2}. \quad (\text{B25})$$

Equation (B25) is what we used in Sec. III B to discuss the impurity-induced localization in the presence of bond disorder.

In the case in which there is a dimer-impurity at sites $j = 1$ and $j = 2$ into an otherwise uniform SSH chain, we see that the interface conditions in Eq. (B22) are substituted by the conditions

$$\begin{aligned}-W\psi_{1,k,+}^< + J_o(\psi_{2,k,+}^> - \psi_{2,k,+}^<) &= 0, \\ J_o(\psi_{k,1,+}^< - \psi_{k,1,+}^>) - W\psi_{2,k,+}^> &= 0.\end{aligned}\quad (\text{B26})$$

with W denoting the corresponding potential strength, Choosing a positive-energy solution as in Eqs. (B20) and (B21), from Eqs. (B26) we obtain the system

equations for r_k and t_k in the form

$$\begin{aligned} & -W \left\{ e^{ik - \frac{i\omega_k}{2}} + r_k e^{-ik + \frac{i\omega_k}{2}} \right\} \\ & + J_o \left\{ e^{2ik + \frac{i\omega_k}{2}} t_k - e^{2ik + \frac{i\omega_k}{2}} - r_k e^{-2ik - \frac{i\omega_k}{2}} \right\} = 0, \\ J_o \left\{ e^{ik - \frac{i\omega_k}{2}} + r_k e^{-ik + \frac{i\omega_k}{2}} - e^{ik - \frac{i\omega_k}{2}} t_k \right\} \\ & - W e^{2ik + \frac{i\omega_k}{2}} t_k = 0. \end{aligned} \quad (\text{B27})$$

Solving for r_k , we now obtain

$$r_k = - \frac{e^{4ik + i\omega_k} W (W + 2J_o \cos(k + \varphi_k))}{J_o^2 + 2e^{i(k + \varphi_k)} J_o W + e^{2i(k + \varphi_k)} (-J_o^2 + W^2)}. \quad (\text{B28})$$

Equation (B28) is what we have used in Sec. III C to discuss the localization effects of dimer disorder in the SSH chain and, in particular, to infer under which conditions we recover the emergence of a mobility edge in the disordered system.

-
- [1] D. J. Thouless, M. Kohmoto, M. P. Nightingale, and M. den Nijs, *Phys. Rev. Lett.* **49**, 405 (1982).
- [2] C. L. Kane and E. J. Mele, *Phys. Rev. Lett.* **95**, 226801 (2005).
- [3] C. L. Kane and E. J. Mele, *Phys. Rev. Lett.* **95**, 146802 (2005).
- [4] B. A. Bernevig, T. L. Hughes, and S.-C. Zhang, *Science* **314**, 1757 (2006).
- [5] C. Nayak, S. H. Simon, A. Stern, M. Freedman, and S. Das Sarma, *Rev. Mod. Phys.* **80**, 1083 (2008).
- [6] M. V. Berry, *Proc. R. Soc. London, Ser. A* **392**, 45 (1984).
- [7] C. Kane, in *Topological Insulators*, Contemporary Concepts of Condensed Matter Science, edited by M. Franz and L. Molenkamp (Elsevier, 2013), Vol. 6, pp. 3–34.
- [8] J. Zak, *Phys. Rev. Lett.* **62**, 2747 (1989).
- [9] R. Resta, *Rev. Mod. Phys.* **66**, 899 (1994).
- [10] C.-S. Lee, I.-F. Io, and H. chung Kao, *Chin. J. Phys.* **78**, 96 (2022).
- [11] M. Atala, M. Aidelsburger, J. T. Barreiro, D. Abanin, T. Kitagawa, E. Demler, and I. Bloch, *Nat. Phys.* **9**, 795 (2013).
- [12] P. W. Anderson, *Phys. Rev.* **109**, 1492 (1958).
- [13] E. Abrahams, P. W. Anderson, D. C. Licciardello, and T. V. Ramakrishnan, *Phys. Rev. Lett.* **42**, 673 (1979).
- [14] F. Pientka, A. Romito, M. Duckheim, Y. Oreg, and F. von Oppen, *New J. Phys.* **15**, 025001 (2013).
- [15] A. Nava, R. Giuliano, G. Campagnano, and D. Giuliano, *Phys. Rev. B* **95**, 155449 (2017).
- [16] Z.-W. Zuo and D. Kang, *Phys. Rev. A* **106**, 013305 (2022).
- [17] J. Li, R.-L. Chu, J. K. Jain, and S.-Q. Shen, *Phys. Rev. Lett.* **102**, 136806 (2009).
- [18] J. C. Flores, *J. Phys.: Condens. Matter* **1**, 8471 (1989).
- [19] H.-L. Wu, W. Goff, and P. Phillips, *Phys. Rev. B* **45**, 1623 (1992).
- [20] B. Ostahie and A. Aldea, *Phys. Lett. A* **387**, 127030 (2021).
- [21] S.-N. Liu, G.-Q. Zhang, L.-Z. Tang, and D.-W. Zhang, *Phys. Lett. A* **431**, 128004 (2022).
- [22] Y. Wu, *arXiv:2209.05981*.
- [23] E. J. Meier, F. A. An, and B. Gadway, *Nat. Commun.* **7**, 13986 (2016).
- [24] B. Gadway, *Phys. Rev. A* **92**, 043606 (2015).
- [25] J.-F. Schaff, Z. Akdeniz, and P. Vignolo, *Phys. Rev. A* **81**, 041604(R) (2010).
- [26] A. J. Heeger, S. Kivelson, J. R. Schrieffer, and W. P. Su, *Rev. Mod. Phys.* **60**, 781 (1988).
- [27] V. Bellani, E. Diez, R. Hey, L. Toni, L. Tarricone, G. B. Parravicini, F. Domínguez-Adame, and R. Gómez-Alcalá, *Phys. Rev. Lett.* **82**, 2159 (1999).
- [28] U. Naether, S. Stützer, R. A. Vicencio, M. I. Molina, A. Tünnermann, S. Nolte, T. Kottos, D. N. Christodoulides, and A. Szameit, *New J. Phys.* **15**, 013045 (2013).
- [29] G. Lindblad, *Commun. Math. Phys.* **48**, 119 (1976).
- [30] E. Braaten, H.-W. Hammer, and G. P. Lepage, *Phys. Rev. A* **95**, 012708 (2017).
- [31] W. Lee, M. Kim, H. Jo, Y. Song, and J. Ahn, *Phys. Rev. A* **99**, 043404 (2019).
- [32] S. Lieu, M. McGinley, and N. R. Cooper, *Phys. Rev. Lett.* **124**, 040401 (2020).
- [33] J. C. Budich, P. Zoller, and S. Diehl, *Phys. Rev. A* **91**, 042117 (2015).
- [34] A. Nava and M. Fabrizio, *Phys. Rev. B* **100**, 125102 (2019).
- [35] A. Nava and M. Fabrizio, *SciPost Phys.* **12**, 014 (2022).
- [36] C. Artiago, A. Nava, and M. Fabrizio, *arXiv:2206.11662*.
- [37] M. B. Plenio and S. F. Huelga, *New J. Phys.* **10**, 113019 (2008).
- [38] D. Manzano, *PLoS ONE* **8**, 1 (2013).
- [39] J. del Pino, J. Feist, and F. J. Garcia-Vidal, *New J. Phys.* **17**, 053040 (2015).
- [40] A. Nava, D. Giuliano, L. Lepori, and M. Rossi, *J. Phys.: Conf. Ser.* **2164**, 012051 (2022).
- [41] H. I. Nurdin, M. R. James, and A. C. Doherty, *SIAM J. Control Optim.* **48**, 2686 (2009).
- [42] F. Verstraete, M. M. Wolf, and J. Ignacio Cirac, *Nat. Phys.* **5**, 633 (2009).
- [43] S. Diehl, A. Micheli, A. Kantian, B. Kraus, H. P. Büchler, and P. Zoller, *Nat. Phys.* **4**, 878 (2008).
- [44] A. W. Schlimgen, K. Head-Marsden, LeeAnn M. Sager, P. Narang, and D. A. Mazziotti, *Phys. Rev. Res.* **4**, 023216 (2022).
- [45] S. Diehl, E. Rico, M. A. Baranov, and P. Zoller, *Nat. Phys.* **7**, 971 (2011).
- [46] M. Goldstein, *SciPost Phys.* **7**, 067 (2019).
- [47] G. Shavit and M. Goldstein, *Phys. Rev. B* **101**, 125412 (2020).
- [48] A. Beck and M. Goldstein, *Phys. Rev. B* **103**, L241401 (2021).
- [49] F. Tarantelli and E. Vicari, *Phys. Rev. A* **105**, 042214 (2022).
- [50] G. Di Meglio, D. Rossini, and E. Vicari, *Phys. Rev. B* **102**, 224302 (2020).
- [51] M. de Leeuw, C. Paletta, and B. Pozsgay, *Phys. Rev. Lett.* **126**, 240403 (2021).
- [52] F. Dangel, M. Wagner, H. Cartarius, J. Main, and G. Wunner, *Phys. Rev. A* **98**, 013628 (2018).
- [53] C. Artiago, F. Balducci, and A. Scardicchio, *Phys. Rev. B* **103**, 214205 (2021).
- [54] P. H. Guimarães, G. T. Landi, and M. J. de Oliveira, *Phys. Rev. E* **94**, 032139 (2016).
- [55] F. Tarantelli and E. Vicari, *Phys. Rev. B* **104**, 075140 (2021).
- [56] V. Popkov and G. M. Schütz, *Phys. Rev. E* **95**, 042128 (2017).

- [57] I. Pižorn, *Phys. Rev. A* **88**, 043635 (2013).
- [58] G. Benenti, G. Casati, T. Prosen, and D. Rossini, *Europhys. Lett.* **85**, 37001 (2009).
- [59] G. Benenti, G. Casati, T. Prosen, D. Rossini, and M. Žnidarič, *Phys. Rev. B* **80**, 035110 (2009).
- [60] A. Nava, M. Rossi, and D. Giuliano, *Phys. Rev. B* **103**, 115139 (2021).
- [61] D. N. Maksimov and A. R. Kolovsky, [arXiv:2207.01943](https://arxiv.org/abs/2207.01943).
- [62] E. H. Lieb, *Phys. Rev. Lett.* **62**, 1201 (1989).
- [63] A. Mielke, *Phys. Lett. A* **174**, 443 (1993).
- [64] P. Phillips and H.-L. Wu, *Science* **252**, 1805 (1991).
- [65] I. Mondragon-Shem, T. L. Hughes, J. Song, and E. Prodan, *Phys. Rev. Lett.* **113**, 046802 (2014).
- [66] H.-P. Breuer and F. Petruccione, *The Theory of Open Quantum Systems* (Oxford University Press, New York, 2002).
- [67] C. Gardiner and P. Zoller, *Quantum Noise* (Springer, Berlin, 2000).
- [68] T. Giamarchi, in *Quantum Physics in One Dimension* (Oxford University Press, New York, 2003).
- [69] D. H. Dunlap, H.-L. Wu, and P. W. Phillips, *Phys. Rev. Lett.* **65**, 88 (1990).
- [70] T. Sedrakyan, *Phys. Rev. B* **69**, 085109 (2004).
- [71] T. Sedrakyan and A. Ossipov, *Phys. Rev. B* **70**, 214206 (2004).
- [72] T. A. Sedrakyan, J. P. Kestner, and S. Das Sarma, *Phys. Rev. A* **84**, 053621 (2011).
- [73] L. Fidkowski, J. Alicea, N. H. Lindner, R. M. Lutchyn, and M. P. A. Fisher, *Phys. Rev. B* **85**, 245121 (2012).
- [74] I. Affleck and D. Giuliano, *J. Stat. Mech.: Theory Exp.* (2013) P06011.
- [75] I. Affleck and D. Giuliano, *J. Stat. Phys.* **157**, 666 (2014).
- [76] A. Bayat, S. Bose, P. Sodano, and H. Johannesson, *Phys. Rev. Lett.* **109**, 066403 (2012).
- [77] C. J. Lambert and M. F. Thorpe, *Phys. Rev. B* **26**, 4742 (1982).
- [78] P. Phillips and H.-L. Wu, *J. Non-Cryst. Solids* **137**, 927 (1991).
- [79] X.-L. Qi, T. L. Hughes, and S.-C. Zhang, *Phys. Rev. B* **78**, 195424 (2008).
- [80] Y. Aihara, M. Hirayama, and S. Murakami, *Phys. Rev. Res.* **2**, 033224 (2020).
- [81] G. W. Semenoff and P. Sodano, *EJTP* **3**, 157 (2006).
- [82] R. Yousefjani and A. Bayat, [arXiv:2209.01337](https://arxiv.org/abs/2209.01337).
- [83] D. Vodola, L. Lepori, E. Ercolessi, A. V. Gorshkov, and G. Pupillo, *Phys. Rev. Lett.* **113**, 156402 (2014).
- [84] D. Giuliano, S. Paganelli, and L. Lepori, *Phys. Rev. B* **97**, 155113 (2018).
- [85] B. Béri and N. R. Cooper, *Phys. Rev. Lett.* **109**, 156803 (2012).
- [86] A. M. Tsvelik, *Phys. Rev. Lett.* **110**, 147202 (2013).
- [87] D. Giuliano and P. Sodano, *Europhys. Lett.* **103**, 57006 (2013).
- [88] D. Giuliano, A. Nava, and P. Sodano, *Nucl. Phys. B* **960**, 115192 (2020).
- [89] D. Giuliano, L. Lepori, and A. Nava, *Phys. Rev. B* **101**, 195140 (2020).
- [90] F. Buccheri, A. Nava, R. Egger, P. Sodano, and D. Giuliano, *Phys. Rev. B* **105**, L081403 (2022).
- [91] D. Giuliano, A. Nava, R. Egger, P. Sodano, and F. Buccheri, *Phys. Rev. B* **105**, 035419 (2022).
- [92] D. Guerci and A. Nava, *Phys. E* **134**, 114895 (2021).